Title
HYPERPINE STRUCTURE OF Dy165 AND SPIN OF Erl63

Author
Stein, Sanford.

Publication Date
1967-12-15

UCRL-17969

cy. 2

University of California

Ernest O. Lawrence Radiation Laboratory

HYPERFINE STRUCTURE OF Dy^{165} AND SPIN OF Er^{163}

Sanford Stein
(Ph.D. Thesis)

December 15, 1967

DISCLAIMER

UCRL-17969

UNIVERSITY OF CALIFORNIA

Lawrence Radiation Laboratory
Berkeley, California

AEC Contract No. W-7405-eng-48

HYPERFINE STRUCTURE OF Dy^{165} AND SPIN OF Er^{163}

Sanford Stein

(Ph.D. Thesis)

December 15, 1967

HYPERFINE STRUCTURE OF Dy^{165} AND SPIN OF Er^{163}

Sanford Stein

Lawrence Radiation Laboratory
University of California
Berkeley, California

ABSTRACT

The atomic beam magnetic resonance flop-in method was used to measure the hyperfine structure of Dy^{165} and the spin of Er^{163}.

The result for the $_{66}Dy^{165}_{99}$ ground state are

$$a = \pm 89.8(7) \text{ MHz}$$

$$b = \mp 1520(30) \text{ MHz}$$

where a and b are the magnetic dipole and electric quadrupole hyperfine interaction constants. The spin was previously measured to be $I = 7/2$. From these values one can calculate the nuclear magnetic dipole moment μ_I and the nuclear electric quadrupole moment Q which are

$$\mu_I(\text{uncorr}) = \mp 0.50(4) \text{ nm}$$

$$Q(\text{uncorr}) = \pm 2.8(3) \text{ barns}$$

These values are in good agreement with that predicted by the strong deformation collective model.

The spin of the ground state of $_{68}Er^{163}_{95}$ is

$$I = 5/2$$

which agrees with the Nilsson state assignment.

The theory underlying the atomic beam method, a description of the technique and equipment used, and a comparison with appropriate theoretical calculations are presented.

I. INTRODUCTION

The field of atomic beams is a little over 50 years old. It had its start in 1911 when Dunoyer (DUN 11) produced directed beams of neutral sodium atoms. The mean free path was much longer than the apparatus so collisions could be ignored. The beam method was used as a tool by Stern and his collaborators to study the Maxwellian distribution, molecular scattering and many other diverse phenomena. This lead to the incorporation of an inhomogeneous magnetic field in the beam path and demonstration of the space grantization of angular momentum, the famous Stern-Gerlach experiment (STE 21). Employing the known technique of two inhomogeneous magnetic fields as polarizer and analyzer, Rabi (RAB 38) made further improvements by incorporating a small oscillating magnetic field to cause a desired transition between levels. This enabled one to concentrate on a single transition rather than on all of the transitions at the same time. A refinement in the configuration of the machine by Zacharias (ZAC 42) to a flop-in type, i.e. where a resonance means an enhancement of the signal rather than a diminishment, lead to an increase in the signal-to-noise ratio. With the advent of radioactive samples and radioactive detection schemes the signal-to-noise became even larger (SMI 51). The basic design of the flop-in atomic beam apparatus used in this experiment is described in Brink's Ph.D. thesis (BRI 57).

Only that part of the theory directly connected with the experiment or of general importance will be covered in this thesis. For more general references there are the review articles "The Measurement of the Nuclear Spin and Static Moments of Radioactive Isotopes" (NIE 57) or "On Atomic Beams" (MAR 62) or the book "Molecular Beams (RAM 56).

II. ATOMIC THEORY

The nonrelativistic Hamiltonian representing a system of N electrons in the field of a nucleus having Z protons can be written as

$$\mathcal{H} = \mathcal{H}_N + \mathcal{H}_{en} + \mathcal{H}_{ee} + \mathcal{H}_{fs} + \mathcal{H}_{hfs} + \mathcal{H}_{other} \tag{2.1}$$

where

$$\mathcal{H}_{en} = \sum_{i=1}^{N} \left(\frac{Pi^2}{2\mu} - \frac{Ze^2}{r_i}\right) \tag{2.2}$$

$$\mathcal{H}_{ee} = \sum_{i>j=1}^{N} \frac{e^2}{r_{ij}} \tag{2.3}$$

$$\mathcal{H}_{fs} = \sum_{i=1}^{N} \xi\,(r_i)\ \bar{\ell}_i \cdot \bar{s}_i \tag{2.4}$$

$\mathcal{H}_N$ represents the internal energy of the nucleus. Since the energy difference between the nuclear ground state and any excited state is very large (keV or MeV) it can be ignored here since one is not dealing with energies sufficient to excite the atom out of its ground state. In fact the energies dealt with here are extremely small, about 1000 MHz (0.00001 eV). $\mathcal{H}_{en}$ is the interaction of the electrons with the nucleus consisting of the kinetic energy of each electron and the Coulomb attraction between each electron and the nucleus. $\mathcal{H}_{ee}$ is the Coulomb repulsion between electrons. $\mathcal{H}_{fs}$, the fine structure, is the interaction between the spin of the electrons and their orbits. $\mathcal{H}_{hfs}$, the hyperfine structure, is the interaction of the nucleus with the electric and magnetic fields generated by the electrons. It will be treated in detail in the next section. $\mathcal{H}_{other}$ are other interactions such as spin-spin, spin-other-orbit, orbit-orbit, etc. which for the present can be ignored due to their small effect.

The eigenvalue equation

$$\mathcal{H}\Psi = E\Psi \tag{2.5}$$

is presently to complicated to be solved analytically. Since $\mathcal{H}_{en} + \mathcal{H}_{ee} > \mathcal{H}_{fs} > \mathcal{H}_{hfs}$ one can break the Hamiltonian into its various parts and approximate a solution by perturbation theory (CON 35) (SLA 60).

III. HYPERFINE STRUCTURE

For the Dysprosium and Erbium isotopes used in the experiment the magnetic octupole moment was too small to be observed so it will be ignored. Thus the hyperfine structure arises from the coupling of the nuclear magnetic moment with the magnetic field of the atom at the position of the nucleus and of the nuclear electric quadrupole moment with the gradient of the electric field at the nucleus.

In general, the energy for a magnetic dipole is

$$\mathcal{H}_{dip} = -\bar{\mu}\cdot\bar{H} \tag{3.1}$$

where $\bar{\mu}$ is the dipole moment and $\bar{H}$ is the magnetic field. Here $\bar{\mu}$ is $\bar{\mu}_I$, the nuclear magnetic moment and $\bar{H}$ is $\bar{H}_N$, the average magnetic field at the nucleus produced by the orbital and spin magnetic moments of the orbital electrons. Thus one has

$$\mathcal{H}_{dip} = -\bar{\mu}_I \cdot \bar{H}_N \tag{3.2}$$

Normally the magnetic dipole moment of the nucleus is treated as a point dipole oriented collinearly with the nuclear angular momentum I which gives

$$\bar{\mu}_I = g_I \mu_0 \bar{I} \tag{3.3}$$

where μ_0 is the Bohr magneton ($\mu_0 = \frac{e\hbar}{2mc} = 0.927 \times 10^{-20}$ erg/G). The magnetic dipole moment μ_I is the expectation value of $\bar{\mu}_I$ in the state $m_I = I$.

The classical expression for the magnetic field at the nucleus due to circulating electrons with permanent magnetic dipole moments is

$$\bar{H}_N = \sum_i \left(-\frac{e}{c}\frac{\bar{r}\times\bar{v}}{r^3} - \frac{\bar{\mu}(\bar{r}\cdot\bar{r}) - 3\bar{r}(\bar{\mu}\cdot\bar{r})}{r^5}\right) \tag{3.4}$$

The sum is over all electrons not in closed shells. Writing in the form of angular momentum operators one gets

$$\bar{H}_N = 2\mu_0 \sum_i \left\langle\frac{1}{r^3}\right\rangle_i \left\{-\bar{\ell} + \bar{s} - \frac{3\bar{r}(\bar{s}\cdot\bar{r})}{r^2}\right\}_i \tag{3.5}$$

where $m\bar{r}\times\bar{v} = \hbar\bar{\ell}$, $\bar{\mu} = -2\mu_0\bar{s}$ and $\bar{j} = \bar{\ell} + \bar{s}$, $(\sum_i \bar{j}_i = \bar{J})$.

It can be shown that (MAR 62)

$$\langle IJFm_F|-\bar{\mu}_I\cdot\bar{H}_N|IJFm_F\rangle = \langle IJFm_F|ah\bar{I}\cdot\bar{J}|IJFm_F\rangle \tag{3.6}$$

which defines the magnetic dipole interaction constant a . Evaluating both sides in the state with the maximum total angular momentum F = I + J and the state with maximum m_F yields

$$a = -\frac{1}{IJ\hbar}\mu_I \langle H_z(0)\rangle_J,\ m_J = J \tag{3.7}$$

For the complex atoms dealt with in the rare earth and transuranic regions of the periodic table, the evaluation of the magnetic field depends on the coupling assumed among the electrons. The coupling used here is that of equivalent electrons of the configuration $(\ell)^n$ coupling to the Hund's rule ground state term of maximum spin S and maximum orbital angular momentum L consistent with the Pauli Exclusion Principle. This calculation is carried out in (MAR 62) where other couplings are also discussed.

$$\langle H_z(0)\rangle = -2\mu_0\left\langle\frac{1}{r^3}\right\rangle\left\{\frac{J(J+1)+L(L+1)-S(S+1)}{2(J+1)} + \right.$$
$$+\frac{2(2L-n^2)}{n^2(2L-1)(2\ell-1)(2\ell+3)}\left[\frac{L(L+1)[J(J+1)+S(S+1)-L(L+1)]}{2(J+1)}\right. \qquad (3.8)$$
$$\left.\left.-\frac{3}{4}\frac{[J(J+1)-L(L+1)-S(S+1)][J(J+1)+L(L+1)-S(S+1)]}{(J+1)}\right]\right\}$$

where n is the number of electrons for less than a half filled shell or the number of holes for more than a half filled shell.

Since $\langle H_z(0)\rangle$ depends only on the orbital electrons it is to a good approximation the same for all isotopes of the same element. Therefore from Eq. (3.7) one can see that

$$\mu_I(2) = \mu_I(1)\frac{a(2)}{a(1)}\frac{I(2)}{I(1)} \text{ or } g_I(2) = g_I(1)\frac{a(2)}{a(1)} \qquad (3.9)$$

This is one of the Fermi-Segrè relations.

The electric quadrupole energy can be expressed as

$$\mathcal{H}_{quad} = -e^2\frac{r_N^2}{r_e^2}\sum_k (-1)^k C_k^{(2)}(\theta_N,\phi_N)\, C_{-k}^{(2)}(\theta_e,\phi_e) \qquad (3.10)$$

where r_e and r_N are respectively the electronic and nuclear radii and $C_k^{(2)}(\theta,\phi) = (4\pi/5)^{1/2} Y_k^2(\theta,\phi)$ are spherical harmonics. One can evaluate the matrix element in the $|IJFm_F\rangle$ representation obtaining

$$\langle IJFm_F|\mathcal{H}_{quad}|IJFm_F\rangle = -\frac{e^2q_JQ}{2IJ(2I-1)(2J-1)}\left[\frac{3}{4}(2\bar{I}\cdot\bar{J})(2\bar{I}\cdot\bar{J}+1)-I(I+1)J(J+1)\right] \qquad (3.11)$$

where $F=I+J$ $\quad 2\bar{I}\cdot\bar{J}=F(F+1)-I(I+1)-J(J+1)$

$$q_J=\langle J,m_J=J|\sum_i\left\langle\frac{1}{r^3}\right\rangle_i (3\cos^2\theta_i-1)|J,m_J=J\rangle \quad \text{(sum over electrons)}$$

$$Q=\langle I,m_I=I|\sum_k r_k^2(3\cos^2\theta_k-1)|I,m_I=I\rangle \quad \text{(sum over protons)}$$

The quantity $-e^2q_JQ$ is called the electric quadrupole coupling constant and is written as hb.

$$b = -e^2q_JQ/h \tag{3.12}$$

The electric field gradient q_J for Hund's rule ground state is also calculated in (MAR 62) where other couplings also are discussed. For $(\ell)^n$ equivalent electrons one gets

$$q_J = \mp\left\langle\frac{1}{r^3}\right\rangle\left[\frac{3(2\bar{J}\cdot\bar{L})(2\bar{J}\cdot\bar{L}-1)-4L(L+1)J(J+1)}{(2L-1)(J+1)(2J+3)}\right]\left[\frac{(2\ell-n^2)}{n(2\ell-1)(2\ell+3)}\right] \tag{3.13}$$

where $\bar{S} = \bar{J}-\bar{L}$ $\quad 2\bar{J}\cdot\bar{L} = J(J+1)+L(L+1)-S(S+1)$

For less than a half filled shell n is the number of electrons and the minus sign is used; for more than a half filled shell n is the number of holes and the positive sign is used.

Since q_J depends only on the orbital electrons, it is to a good approximation the same for all isotopes of the same element. Therefore from Eq. (3.12) one can see that

$$Q(2) = Q(1)\,\frac{b(2)}{b(1)} \tag{3.14}$$

This is the second Fermi-Segrè relation.

If λ is the order of the moment, then the parity of the electric moment is $(-1)^{\lambda}$ and that of the magnetic moment is $(-1)^{\lambda+1}$ so that only even electric moments (electric quadrupole) and odd magnetic moments (magnetic dipole) can exist. Let χ_λ represent either type of moment of order λ and Ψ_I a state vector with angular momentum I and $\int \Psi_I^* \Psi_I dV \neq 0$.

$$\int \Psi_I^* \chi_\lambda \Psi_I dV \neq 0 \tag{3.15}$$

$\chi_\lambda \Psi_I$ can have angular momentum from $|\lambda-I|$ to $\lambda+I$ but for Eq. (3.15) to exist it must have angular momentum I. This means that it must be possible to add I and λ vectorally to form I or that $2I \geq \lambda$. Therefore an atom with spin 1/2 can only have a magnetic dipole moment, an atom with spin 1 can have only a magnetic dipole moment and an electric quadrupole moment, etc.

The existence of a quadrupole moment means that the charge distribution is not spherically symmetric but a nucleus with spin 0 or 1/2 which can't possess a static electric quadrupole moment is not necessarily spherical. If the quadrupole moment is positive one has a prolate (cigar shaped) charge distribution, if negative an oblate (disc shaped) distribution.

One now has the Hamiltonian

$$\mathcal{H} = ah\bar{I}\cdot\bar{J} + \frac{bh}{2I(2I-1)J(2J-1)}\left[3(\bar{I}\cdot\bar{J})^2+3/2(\bar{I}\cdot\bar{J})-I(I+1)J(J+1)\right] \qquad (3.16)$$

which is true in zero external field. It can be rewritten in terms of b/a as

$$\mathcal{H}' = \bar{I}\cdot\bar{J} + b/a\,\frac{1}{2I(2I-1)J(2J-1)}\left[3(\bar{I}\cdot\bar{J})^2+3/2(\bar{I}\cdot\bar{J})-I(I+1)J(J+1)\right] \qquad (3.17)$$

which for a given I and J is a series of linear equations for the various F's. F can take on values from $|I-J|$ to $I+J$. Eq. (3.17) has been solved on a digital computer for various I's and J's and written up in (BAK 60). One can roughly calculate and plot the lines for various F values manually as has been done in Figs. VI-4 and VI-17 for Dy^{165} and Er^{163}. This gives one the zero field level ordering of the various F levels versus b/a.

If one now puts the atom in an external magnetic field Eq. (3.1) again applies. This time one gets

$$\mathcal{H}_{ext} = -\bar{\mu}_J\cdot\bar{H}_{ext} - \bar{\mu}_I\cdot\bar{H}_{ext} \qquad (3.18)$$

where μ_I is given by Eq. (3.3) and $\bar{\mu}_J$ is similar. It should be noted that μ_I is a thousand times smaller than μ_J since one is dealing with the proton mass rather than the electron mass ($\frac{m}{M} = \frac{1}{1836}$). Unless one goes up to very high fields the μ_I term contributes very little so that it usually can be ignored. This is the reason why μ_I is usually calculated from a .

If one combines Eqs. (3.16) and (3.18) one has the hyperfine Hamiltonian including an external magnetic field.

$$\mathcal{H} = ah\bar{I}\cdot\bar{J} + \frac{bh}{2I(2I-1)J(2J-1)}\left[3(\bar{I}\cdot\bar{J})^2+3/2(\bar{I}\cdot\bar{J})-I(I+1)J(J+1)\right]$$

$$-g_J\mu_0\bar{J}\cdot\bar{H}_{ext} - g_I\mu_0\bar{I}\cdot\bar{H}_{ext} \qquad (3.19)$$

If a and b are zero one has the normal Zeeman splitting which is linear with magnetic field. The existence of a and b causes a deviation from the Zeeman lines. To obtain values for a and b it is necessary to use an external magnetic field of sufficient strength to cause large deviations from the a=b=0 lines. One can solve Eq. (3.19) exactly in both the low and high field regions but in the intermediate field the Hamiltonian is much too complicated to be solved unless J=1/2 or I=1/2. One is thus forced to solve Eq. (3.19) numerically and computer programs have been written (ZUR 64).

Since one measures transitions between levels, a and b , which determine the absolute energies of the various levels, are of little interest at low fields. At low fields one can determine I and J. In a weak external field I and J are tightly coupled together to form the resultant F. I and J precess around F and F precesses around the field direction as shown in Fig. III-1. So at low fields one has

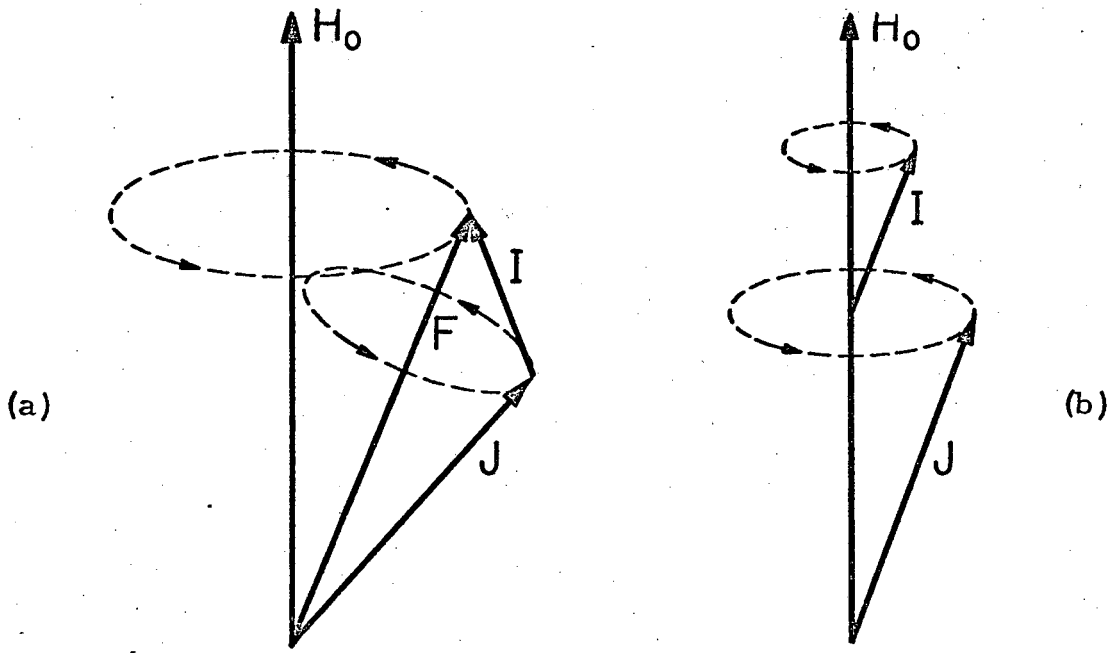

Fig. III-1. The precession of $\bar{I}$ and $\bar{J}$ in the presence of (a) a weak magnetic field, and (b) a strong magnetic field.

$$\mathcal{H}_{\ell f} = -g_J \mu_0 \frac{\overline{J}\cdot\overline{F}\ \ \overline{F}\cdot\overline{H}_{ext}}{\overline{F}\cdot\overline{F}}$$

where $\langle IJFm_F|\overline{J}\cdot\overline{F}|IJFm_F\rangle = \frac{F(F+1)+J(J+1)-I(I+1)}{2}$

$$\langle IJFm_F|\overline{F}\cdot\overline{H}_{ext}|IJFm_F\rangle = m_F H_{ext}$$

So

$$\mathcal{H}_{\ell f} = -g_J \mu_0 \frac{F(F+1)+J(J+1)-I(I+1)}{2F(F+1)} m_F H_{ext} = -g_F \mu_0 m_F H_{ext} \qquad (3.21)$$

Since the photon only has one quantum of angular momentum, m_F can only change by one so the transition frequency is

$$\nu = -\frac{g_J \mu_0 H_{ext}}{h} \frac{F(F+1)+J(J+1)-I(I+1)}{2F(F+1)} \qquad (3.22)$$

As one goes to higher fields one finds that Eq. (3.22) no longer gives the correct transition frequency. One can solve Eq. (3.19) by perturbation theory where $\mathcal{H}_0$, the zero field part, is given by Eq. (3.16) and the perturbation part $\mathcal{H}'$ is given by Eq. (3.18). In the F m representation one has

$$W = W^o_{Fm} + W^1_{Fm} + W^2_{Fm} + \ldots$$

where the superscripts refer to the order of the perturbation and

$$W^o_{Fm} = \langle Fm|\mathcal{H}_0|Fm\rangle = W^o(F,m)$$

$W^1_{Fm} = \langle Fm|\mathcal{H}'|Fm\rangle$ [this is what was obtained in Eq. (3.21)]

$$W^2_{Fm} = \frac{|\langle Fm|\mathcal{H}'|F-1,m\rangle|^2}{W^o_{Fm} - W^o_{F-1,m}} \quad \text{for the highest F state}$$

$$W^2_{Fm} = \frac{|\langle Fm|\mathcal{H}'|F+1,m\rangle|^2}{W^\circ_{Fm} - W^\circ_{F+1,m}} + \frac{|\langle Fm|\mathcal{H}'|F-1,m\rangle|^2}{W^\circ_{Fm} - W^\circ_{F-1,m}} \quad \text{for other F states}$$

Using

$$\langle Fm|\bar{J}\cdot\bar{H}|F-1,m\rangle = -H\sqrt{F^2-m^2}\sqrt{\frac{[F^2-(I-J)^2][(I+J+1)^2-F^2]}{4F^2(4F^2-1)}}$$

$$\langle Fm|\bar{J}\cdot\bar{H}|F+1,m\rangle = -H\sqrt{(F+1)^2-m^2}\sqrt{\frac{[(F+1)^2-(I-J)^2][(I+J+1)^2-(F+1)^2]}{4(F+1)^2[4(F+1)^2-1]}}$$

and defining

$$\Delta\nu_{F,F-1} = \frac{W^\circ_F - W^\circ_{F-1}}{h} \tag{3.23}$$

$$\delta\nu_F = \frac{W^2(F,m) - W^2(F,m-1)}{h} = \frac{W(F,m) - W(F,m-1)}{h} - \nu \tag{3.24}$$

one gets

$$\Delta\nu_{F,F-1} = \frac{W^\circ(F,m) - W^\circ(F-1,m)}{h} = aF + b\,\frac{3F^3 - 3F[I(I+1)+J(J+1)] + 3/2F}{2I(2I-1)J(2J-1)} \tag{3.25}$$

$$\nu = \frac{W(F,m) - W(F,m-1)}{h} = \frac{\mu_0 g_J H}{h}\left[\frac{F(F+1)+J(J+1)-I(I+1)}{2F(F+1)}\right] \text{ [same as Eq. (3.22)]} \tag{3.26}$$

for the highest F state, $F_{max} = I+J$

$$\delta\nu(F_{max}) = -\frac{\nu^2}{\Delta\nu_{F,F-1}}\left\{\frac{[F^2-(I-J)^2][(I+J+1)^2-F^2][m^2-(m-1)^2](F+1)^2}{(4F^2-1)[F(F+1)+J(J+1)-I(I+1)]^2}\right. \tag{3.27}$$

for other F states

$$(F) = -\frac{\nu^2}{\Delta\nu_{F,F+1}} \left\{\frac{[(F+1)^2-(I-J)^2][(I+J+1)^2-(F+1)^2][m^2-(m-1)^2]F^2}{[4(F+1)^2-1][F(F+1)+J(J+1)-I(I+1)]^2}\right\}$$

$$+\frac{\nu^2}{\Delta\nu_{F,F-1}} \left\{\frac{[F^2-(I-J)^2][(I+J+1)^2-F^2][m^2-(m-1)^2](F+1)^2}{(4F^2-1)[F(F+1)+J(J+1)-I(I+1)]^2}\right\} \qquad (3.28)$$

$\delta\nu$ is the difference between the actual measured frequency and the calculated frequency ν for a=b=0, i.e. $\delta\nu$ is the deviation.

To use the perturbation equations one would calculate $\Delta\nu_{F,F-1}$ from Eq. (3.27) and $\Delta\nu_{F,F+1}$ from Eq. (3.28) and solve Eq. (3.25) as two linear simultaneous equations for a and b . To determine the proper transition frequency for a higher field one would use Eqs. (3.26), (3.27) and (3.28) to calculate the deviations $\delta\nu$. The equations don't give very good results so their main use is in approximating the deviations at moderate fields before sufficient shift has occurred to warrant the use of the computer programs. From Eqs. (3.27) and (3.26) one gets

$$\delta\nu(H_1) = C\nu^2(H_1) = KH_1^2 \qquad (3.29)$$

where H is the magnetic field. So for a higher field to second order one has

$$\delta\nu(H_2) = \delta\nu(H_1)\frac{H_2^2}{H_1^2} \qquad (3.30)$$

The frequency used in the experiment is $\nu + \delta\nu$, the linear term plus the deviation. As an example of the accuracy of Eq. (3.30) the deviations are given in Table III-1 for data taken from Table VI-1 for Dy^{165} and from Table VI-2 for Er^{163}. As can be seen the results are not too good.

Table III-1. Deviations Using Perturbation Theory

Field In Gauss	Measured Deviation In MHz	$\delta\nu_2$* In MHz	Transition	Isotope
30	0.23		α	Dy^{165}
50	0.95	0.64	α	"
100	3.90	3.80	α	"
220	19.90	18.9	α	"
30	0.08		β	"
50	0.56	0.22	β	"
100	2.05	2.14	β	"
220	12.82	9.94	β	"
20	1.50		α	Er^{163}
50	4.90	4.16	α	"
130	14.60	33.1	α	"

*$\delta\nu_2 = \delta\nu_1 \frac{H_2^2}{H_1^2}$ where H_1 and $\delta\nu_1$ are the field and deviation from the line above.

To get good values for a and b one must use the computer programs. If one goes to large enough magnetic fields, the $\bar{\mu}_I \cdot \bar{H}$ term in Eq. (3.19) becomes important and one can determine μ_I and its sign directly. Often one is only interested in accuracies of 1% in the hyperfine constants so only the magnitude of μ_I is obtainable from a . Unless one goes to a high magnetic field only the magnitudes and relative sign of a and b are obtainable. The absolute sign is usually inferred from theoretical considerations.

IV. NUCLEAR MODELS

From the data collected in the past on nuclear ground state properties, the following generalizations have been made:

1. The ground state of all nuclei with an even number of protons and of neutrons [even-even] has zero angular momentum (spin) and even parity.

2. In nuclei consisting of an even number of $\binom{\text{neutrons}}{\text{protons}}$ and an odd number of $\binom{\text{protons}}{\text{neutrons}}$, [odd A], the ground state properties are determined by the $\binom{\text{protons}}{\text{neutrons}}$ alone and the nuclei have half integral spin. The spin of a single proton or neutron is $1/2\hbar$.

3. Nuclei with both an odd number of protons and neutrons [odd-odd] have integral spins.

4. Nuclei that contain 2, 8, 20, 28, 50, 82 or 126 protons and or neutrons are particularly stable. These numbers were called "magic numbers" since they had this exceptional stability characteristic which at the time couldn't be explained.

One possible reason why the magic numbers were not obvious was that for the atomic case the spin-orbit coupling plays an unimportant role, it causes a splitting of the levels $j = \ell \pm 1/2$ which is small compared to the energy between levels of different ℓ. But in the nuclear case, it is the reason for the magic numbers. The splitting is so large that it causes changes in the groupings as shown in Fig. IV-1. With the incorporation of the spin-orbit interaction Mayer and independently Haxel, Jenson and Shell in 1950 were able to account for the observed magic numbers and many other nuclear properties (MAY 55). Their theory is called the Shell Model. Nucleons may be considered as

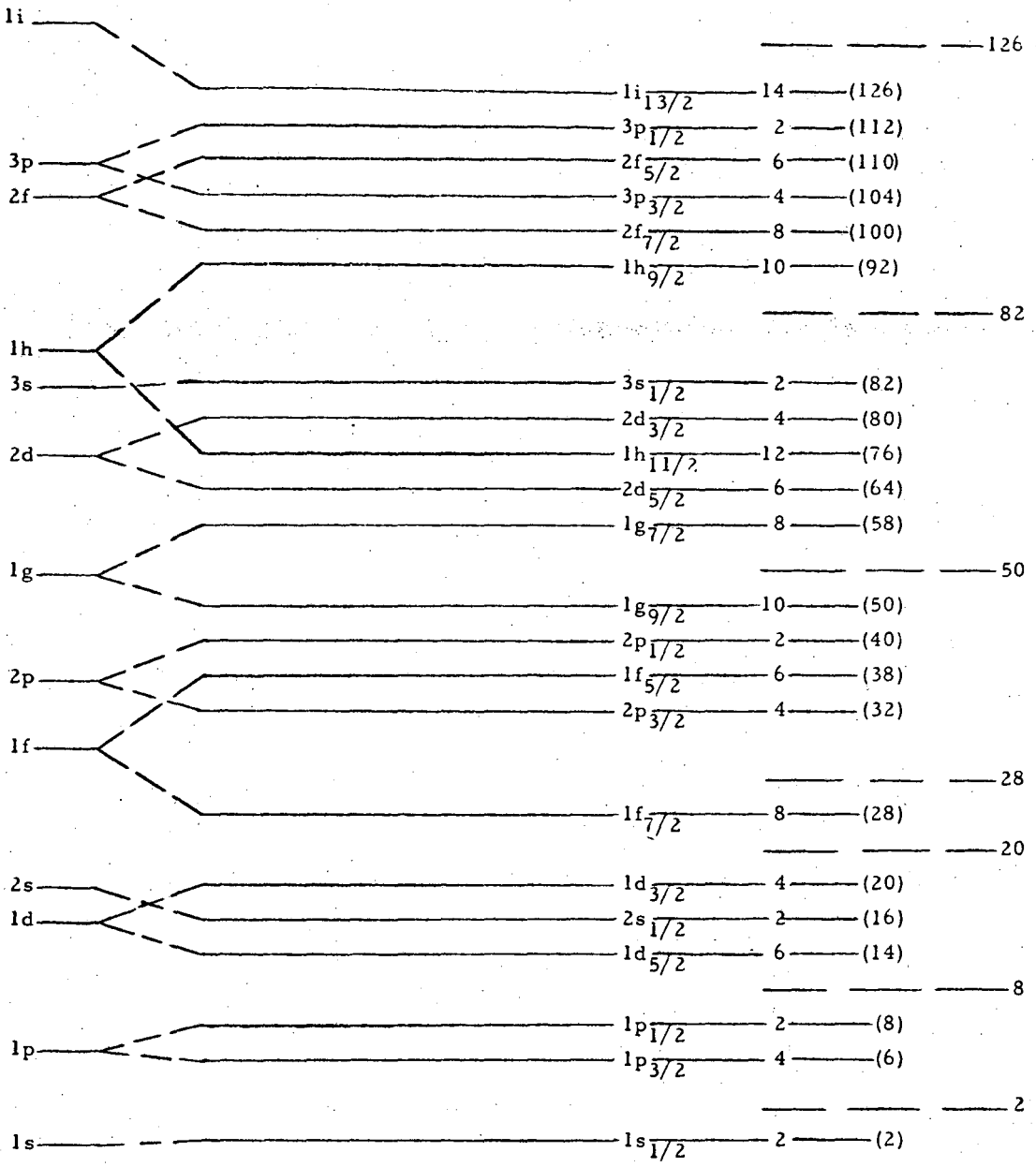

MU-17154

Fig. IV-1. Shell model single-particle energy levels (spin-orbit and Coulomb energy terms included).

occupying states of binding, characteristic of independent particle motion in the average nuclear field.

The observed quadrupole moments of odd-A nuclei in the rare earth region and electric quadrupole radiation (E2) transition rates in even-even nuclei are considerably larger than those predicted by the Shell model. Other models were formulated. The unified model of Bohr and Mottelson (BOH 53) has cleared up some of the difficulties. The large mass of the atomic nucleus, as compared with electrons' mass, had made it possible, to a first approximation, to treat the atomic field as a static quantity; but in the nuclear case, the dynamic aspects of the field associated with the collective oscillations of the structure, as a whole, must be expected to play an essential role. This theory has been refined by Nilsson (NIL 55) and Mottelson and Nilsson (MOT 59) and is usually called the collective model.

Near closed shells (magic numbers) the nuclear shape is spherically symmetric (no deformation) and one has essentially the Shell model with possible collective vibrational motion. Further from the closed shells the nucleus acquires a slight deformation and the coupling between the collective modes and the individual particle modes of motion may lead to a very complicated structure of nuclear states. Still further from closed shells the situation again simplifies. The nucleus has a large deformation with a resulting stability in shape and orientation. Only in the case of large deformation is it possible to separate the nuclear motion into an intrinsic nuclear motion relative to the deformed but fixed nuclear field, a collective rotational motion and a vibrational motion.

For large deformation the magnetic moment is given by Nilsson (NIL 55) for $I \neq 1/2$ as

$$\mu = \frac{I}{I+1}\left\{(g_\delta - g_\ell)\frac{1}{2}\sum_i (a^2_{\ell,\Omega-1/2} - a^2_{\ell,\Omega+1/2}) + g_\ell I + g_R\right\}$$

where the gyromagnetic ratios g_δ, and g_ℓ, and g_R are

$$g_\ell = \begin{Bmatrix}1\\0\end{Bmatrix} \text{ for a free } \begin{Bmatrix}\text{proton}\\\text{neutron}\end{Bmatrix} \text{ and } g_\delta = \begin{Bmatrix}+5.587\\-3.826\end{Bmatrix} \text{ for a free } \begin{Bmatrix}\text{proton}\\\text{neutron}\end{Bmatrix}$$

and for that associated with the surface angular momentum $g_R = Z/A$. The $a_{\ell,\Omega\pm1/2}$'s are the mixing coefficients and are tabulated for various values of δ (the deformation) in Nilsson's articles.

The intrinsic quadrupole moment is given by

$$Q_0 = \frac{4}{5} ZR^2\delta(1+\frac{2}{3}\delta) \tag{4.2}$$

where R is to be taken equal to the radius of charge of the nucleus or $R = 1.2 \times 10^{-13} A^{1/3}$ cm. The relation (projection factor) between the measured quadrupole moment Q and the intrinsic quadrupole moment Q_0 for the ground state is

$$Q = \frac{I(2I-1)}{(I+1)(2I+3)} Q_0 \tag{4.3}$$

Figure IV-2 is from (MOT 59) and is "Single Particle Levels for odd-N nuclei in the region 82<N<126". The numbers alongside the levels, i.e. 7/2 + [633], are the asymtotic Nilsson orbital assignments, Ω, parity $[Nn_3\Lambda]$ where Ω is the spin, N the total harmonic oscillator quantum number, $(-1)^N$ = parity, n_3 is the oscillator quantum number along the Z' axis and Λ is the orbital quantum number. From analogy with $j=\ell+\delta$, $\delta = \pm1/2$ one here has $\Omega = \Lambda + \Sigma$ where $\Sigma = \pm1/2$.

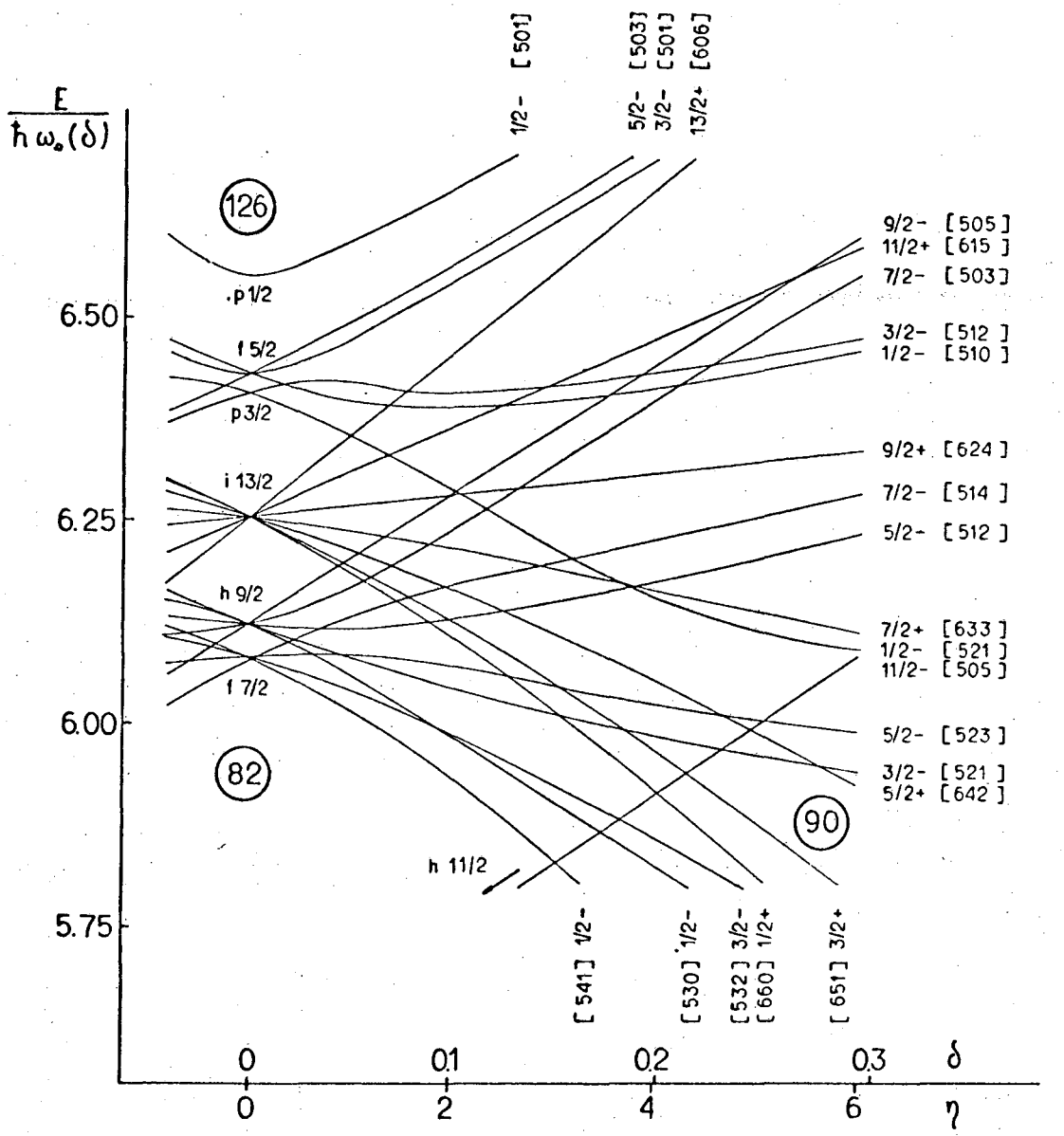

Fig. IV-2. Single particle levels for odd-N nuclei in the region 82<N<126.

V. EXPERIMENTAL TECHNIQUE

The atomic beam machine used in this experiment is described in Brink's thesis (BRI 57). The machine is now buried somewhere in Nevada. The background radiation emitted by the machine, the amount of radioactive waste in the machine and the difficulties in repairing anything, since everything was inside a welded can, made continued use of the machine a dangerous health hazard. Figure V-1 is a picture of the back end of the machine showing the lead shield around the oven chamber and the shielded cave with manipulators while Fig. V-2 shows the front end and button loaders.

The machine is of the flop-in type, where a resonance is given by an enhancement of the signal. It consists of a source of atoms, three magnetic fields, assorted collimating slits, a stop wire, a detector and assorted vacuum pumps as shown schematically in Fig. V-3.

For the isotopes used in this experiment either tantalum or tungsten ovens and oven-liners were used. Oven, oven-liner, oven support and samples from which Dy^{165} and Er^{163} were made are shown in Fig. V-4. For Dy^{165} a chunk of Dysprosium was sealed in a quartz tube under helium and sent to a neutron reactor. Upon its return the quartz tube was opened in a special shielded cave and the sample was dropped into the cave attached to the beam machine where tongs were used to put it into the oven. The oven loader was put into the beam machine by hand. For Er^{163}, four disks of Holmium were placed in a target holder as shown in Fig. VI-8 and sent to the cyclotron. Upon their return the disks were put into the oven. The oven was heated by electron bombardment to produce a beam of atoms.

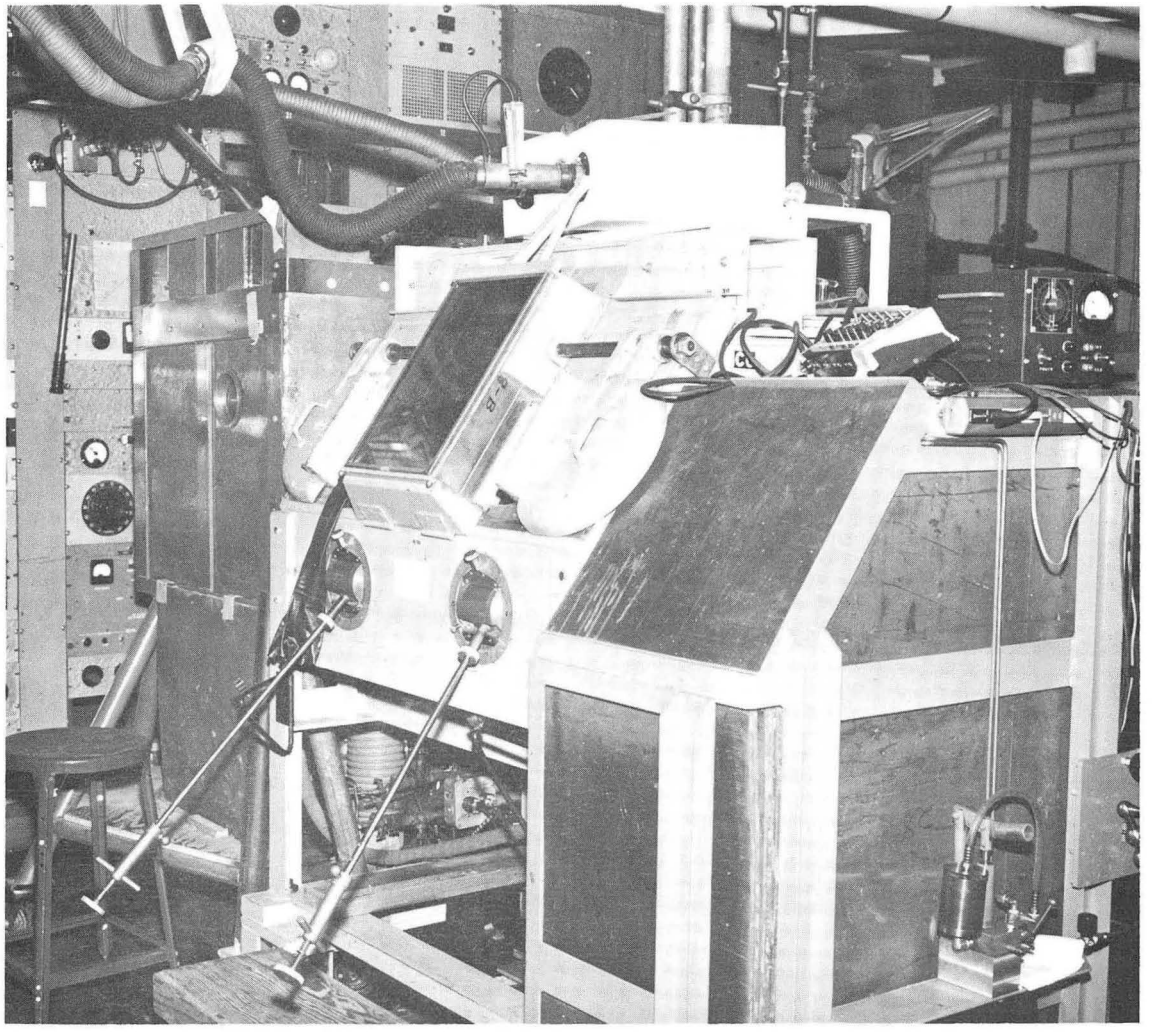

XBB 678-5013

Fig. V-1. Rear of atomic beam machine showing the lead shield around the oven chamber and the shielded cave with manipulators.

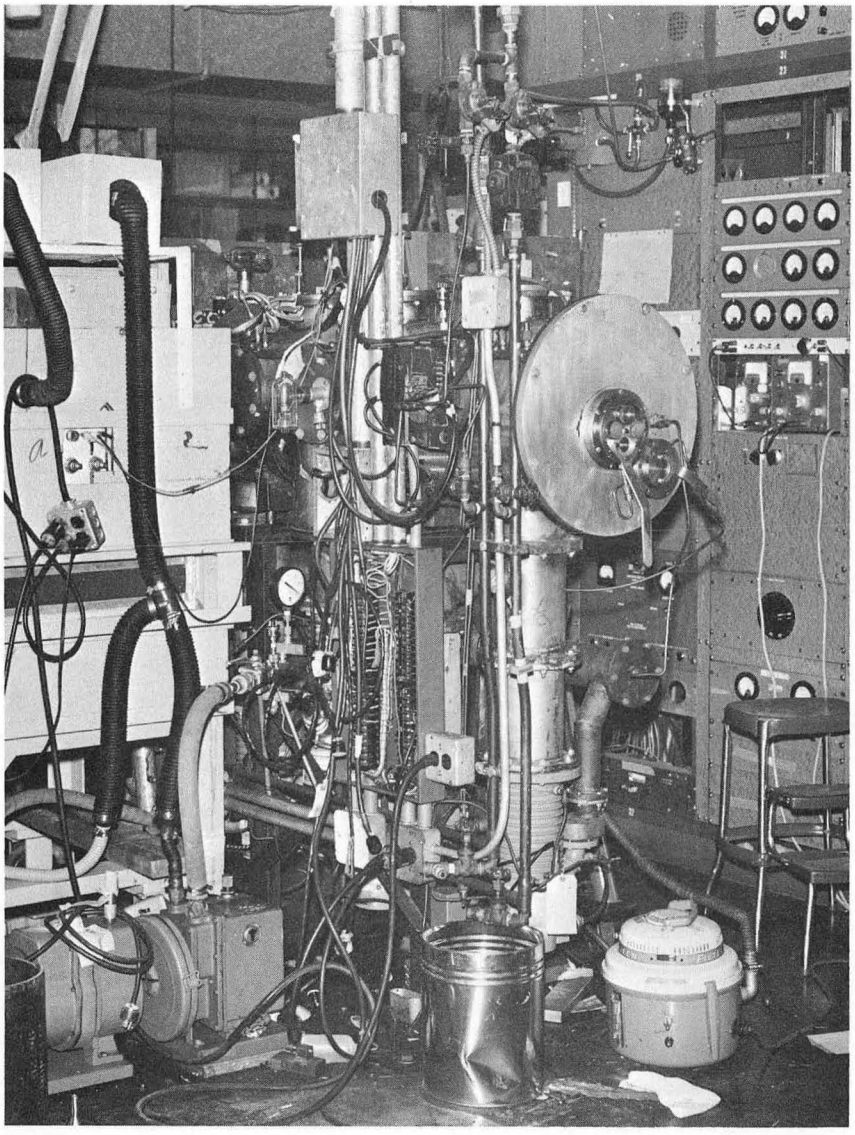

XBB 678-5021

Fig. V-2. Front of atomic beam machine showing back of shielded cave and button loaders.

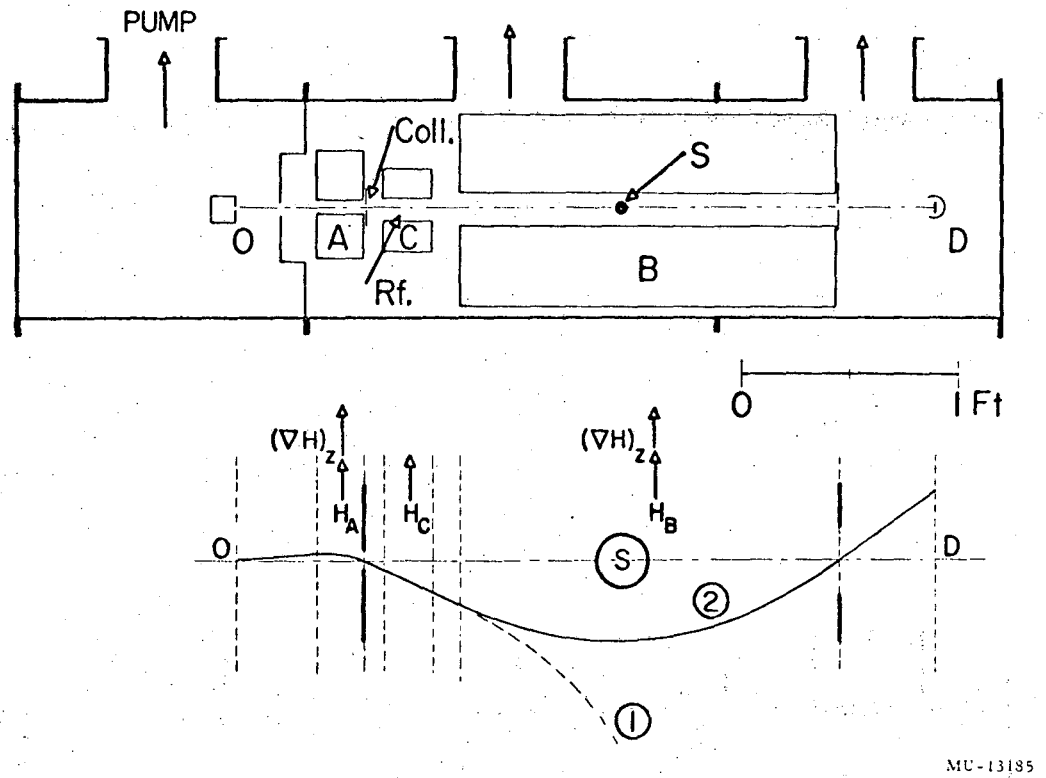

Fig. V-3. Schematic representation of a flop-in atomic beam machine

O = oven

S = Stop wire

D = Detector

① = Path of nonresonance atoms

② = Path of resonance atoms

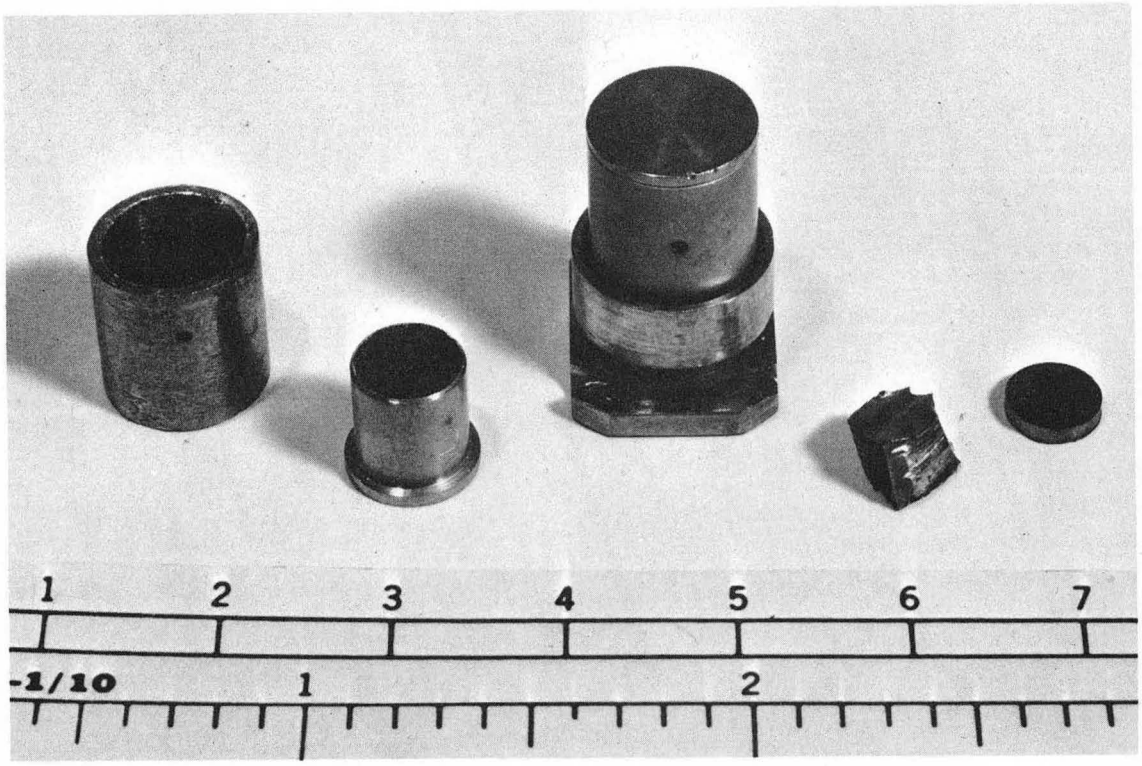

XBB 6711-6665

Fig. V-4. Oven, oven liner, oven mounted on oven support, chunk of Dy and disk of Ho.

The emitted atoms go through a very large inhomogeneous magnetic field, the A region, where they are deflected. The force is given by

$$F = -\nabla\mathcal{H} = -\frac{\partial\mathcal{H}}{\partial H}\frac{\partial H}{\partial Z} = \mu_{eff}\frac{\partial H}{\partial Z} \tag{5.1}$$

where $\mathcal{H}$ is given by Eq. (3.19), H is the magnetic field and Z is the direction of the magnetic field and gradient. The atoms then enter a uniform homogeneous magnetic field, the C region, where a r.f. field can induce transitions. They then go through another very large inhomogeneous magnetic field, the B region, where those atoms not undergoing the correct transitions are further deflected so that they hit the sides of the magnet and are removed from the beam as depicted by trajectory ① of Fig. V-3. Those atoms that have undergone the correct transition are refocused on the detector as shown by trajectory ②.

If the fields and gradients in the A and B regions are the same then for the atoms to be refocused

$$\mu_{eff}(A) = -\mu_{eff}(B) \tag{5.2}$$

where

$$\mu_{eff} = g_J\mu_0 m_J + g_I\mu_0 m_I \approx g_J\mu_0 m_J \tag{5.3}$$

since $|g_J| >> |g_I|$ and one is in the high field or Pashen-Back region. Therefore, the explicit refocusing condition is

$$m_J(A) = -m_J(B) \tag{5.4}$$

The stop wire "S" prevents atoms that are not sufficiently deflected, such as those in the high velocity tail of the Maxwellian distribution, or those that are not deflected at all, the zero moment atoms, i.e. those

with $m_J = 0$, from reaching the detector and contributing a high background.

The hairpin, located in the center of the C field, is the means by which transitions are induced. One applies a r.f. frequency ν to the hairpin and if

$$\nu = \frac{(E_1 - E_2)}{h} \tag{5.5}$$

one can induce transitions between levels E_1 and E_2. The hairpin can induce π (r.f. field perpendicular to C field) transitions and if rotated 90°, σ (r.f. field parallel to C field) transitions. In a weak field the π transitions are

$$\Delta F = \pm 1,\ 0 \text{ with } \Delta m_F = \pm 1 \tag{5.6}$$

while the σ transitions are

$$\Delta F = \pm 1 \text{ with } \Delta m_F = 0 \tag{5.7}$$

For J integral, one must have $\Delta m_J = \pm 2$ for refocusing. The double quantum transitions for weak fields become for π transitions

$$\Delta F = 0,\ \Delta m_F = \pm 2,\ \Delta m_I = 0,\ \Delta m_J = \pm 2 \tag{5.8}$$

and

$$\Delta F = \pm 1,\ \Delta m_F = \pm 1,\ \Delta m_I = \mp 1,\ \Delta m_J = \pm 2 \tag{5.9}$$

The transition in Eq. (5.8) is the one that is used for the spin search and most other measurements.

From Eq. (3.19) it can be seen that the energy levels are magnetic field dependent so one must be able to set the value of the C field very accurately. This is accomplished by having a calibration isotope whose

field versus frequency dependence is known. Stable potassium (K^{39}) was used because it can be detected with a hot wire. Since the ionization potential of K is less than the work function of the tungsten hot wire, K atoms that hit the wire are boiled off as ions and accelerated to a collector plate where the resulting ion current is measured with an electrometer. The field is checked periodically to see that it has not drifted. The K^{39} is in a separate oven that can be lowered infront of the source oven for calibration purposes.

The detector for the radioactive sources are freshly flamed platinum foils which are shown in Fig. V-5. The atoms that make it down the length of the machine strike and stick to the Pt foil. After exposure the foils are taken out of the beam machine and counted in an appropriate counter. For the isotopes used in this experiment, a continuous flow methane β counter was used since the isotopes either decayed by electron emission or capture.

Two types of exposures were made during the experiment. The first, called a direct beam, is used to normalize the beam intensity. It is a one minute exposure with the stop wire out of the way. The second, called a resonance, is taken with the stop wire in the beam path and lasts for five minutes. The normal procedure is to take a direct beam followed by a resonance and then another direct beam to see that the beam intensity has not changed. The values for the resonance curves plotted in section VI are given by

$$\%D.B. = \frac{\text{resonance counts/min} - \text{average counter background/min}}{\text{average of direct beam counts/min taken before and after resonance}} \times 100 \quad (5.10)$$

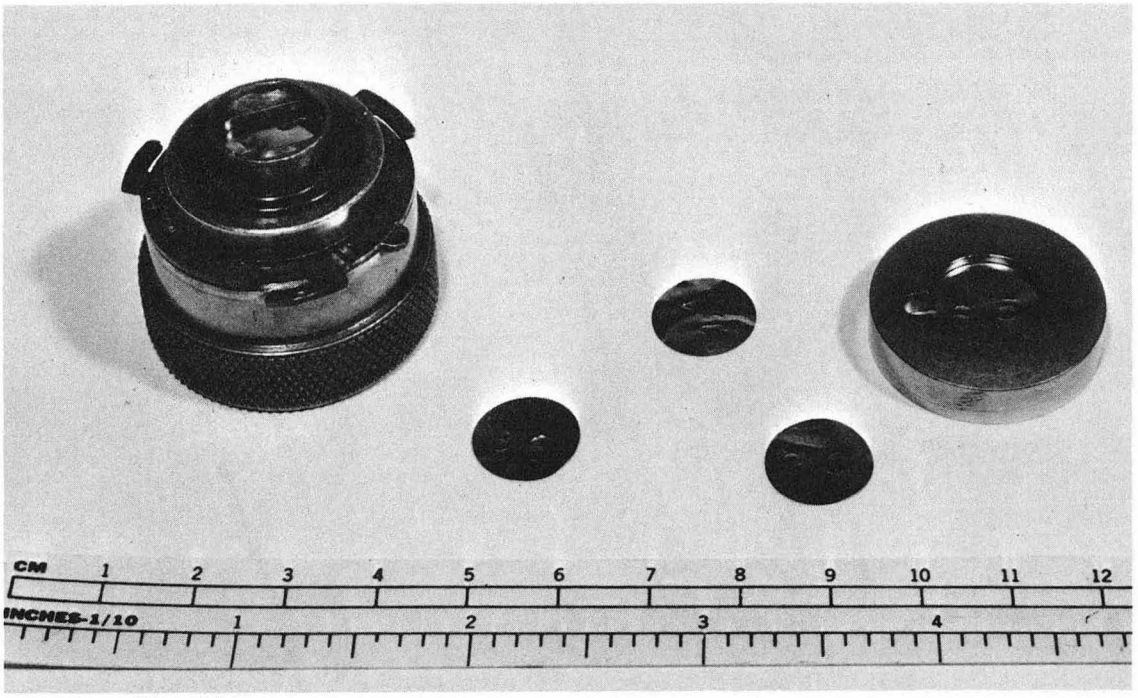

XBB 6711-6664

Fig. V-5. Platinum foils (0.001 in) shown with beam machine button holder and beta counter holder.

The resonance exposures were usually counted for ten minutes while the direct beams were counted for five minutes. This entailed the use of three counters simultaneously. The counters are shown in Fig. V-6 and the foil holders in Fig. V-5. The counter background is about 1 count/min.

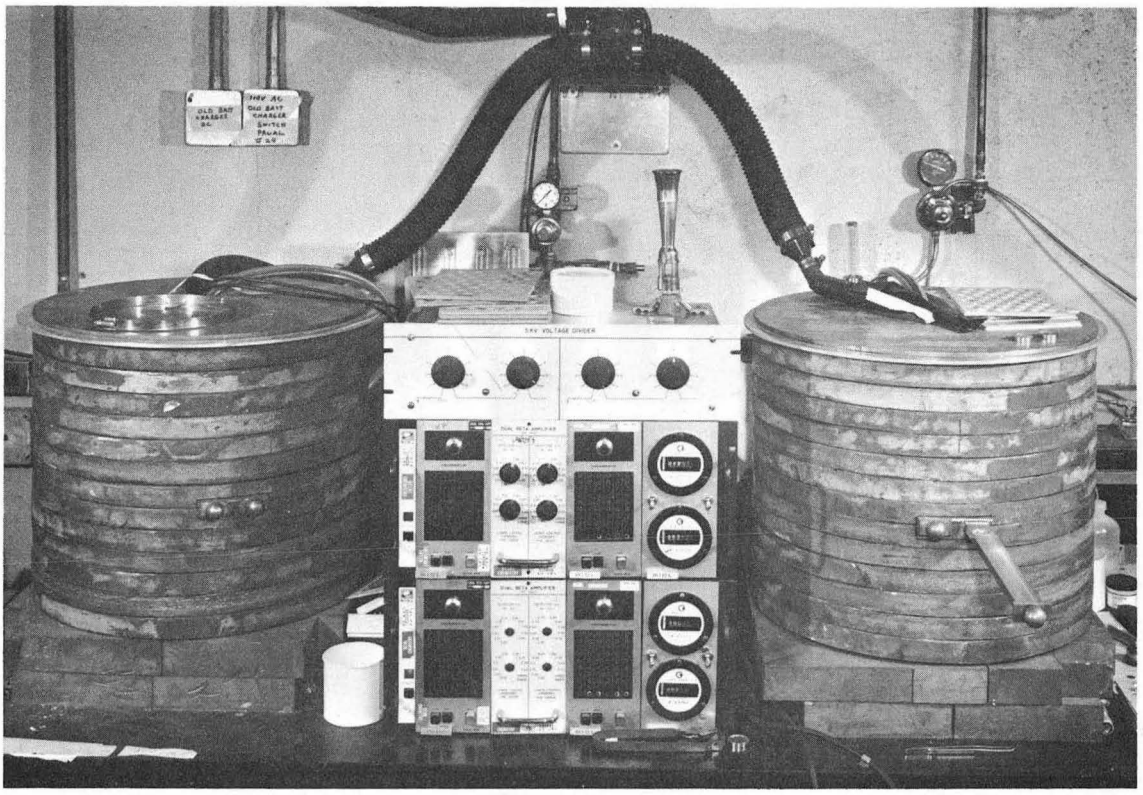

XBB 6711-6662

Fig. V-6. Beta counters and associated electronics.

VI. EXPERIMENTAL RESULTS

A. Hyperfine Structure of Dysprosium-165

1. Introduction

The spin of Dy^{165} was measured to be I = 7/2 by Cabezas (CAB 60). Dy^{165} has a half-life of 2.3 hours, decaying by β^- emission to stable Ho^{165}. Natural dysprosium metal (28% of Dy^{164}) was irradiated for five minutes in a nuclear reactor at the Lawrence Radiation Laboratory at Livermore at a neutron flux of about 1×10^{13} $sec^{-1}cm^{-2}$ to produce Dy^{165} by thermal neutron capture by Dy^{164}. As is evident from Fig. VI-1 only Dy^{165} was produced in detectable amounts. The decay curve is a straight line for eight hours ($\sim$ three half-lives). The sample was placed in a Ta or W oven and oven liner and heated by electron bombardment until a satisfactory beam was obtained. About 100 watts of heating was necessary. Beams were stable and lasted about four hours, by which time all of the approximately 1/2 gram sample was evaporated out of the oven. As soon as one obtained a direct beam in excess of a hundred counts per minute one could start taking data since individual atoms were produced from the beginning of the run. Dy^{166} is even-even and thus having no nuclear spin was used to determine g_J to high accuracy, $g_J = -1.24166(7)$ (SMI 61).

Dysprosium has a $^5I_8$ ground state arising from a $4f^{10}6s^2$ configuration. With a spin of 7/2, there are 136 Zeeman sublevels in the beam, giving rise to eight Zeeman flop-in resonances as shown in Fig. VI-2. Six of the eight transitions yielded high resonances at 20 Gauss (>15%) while the seventh (F = 11/2) resonance was smaller (6%) and the eighth (F = 9/2) even smaller. A possible explanation for this might be that for the

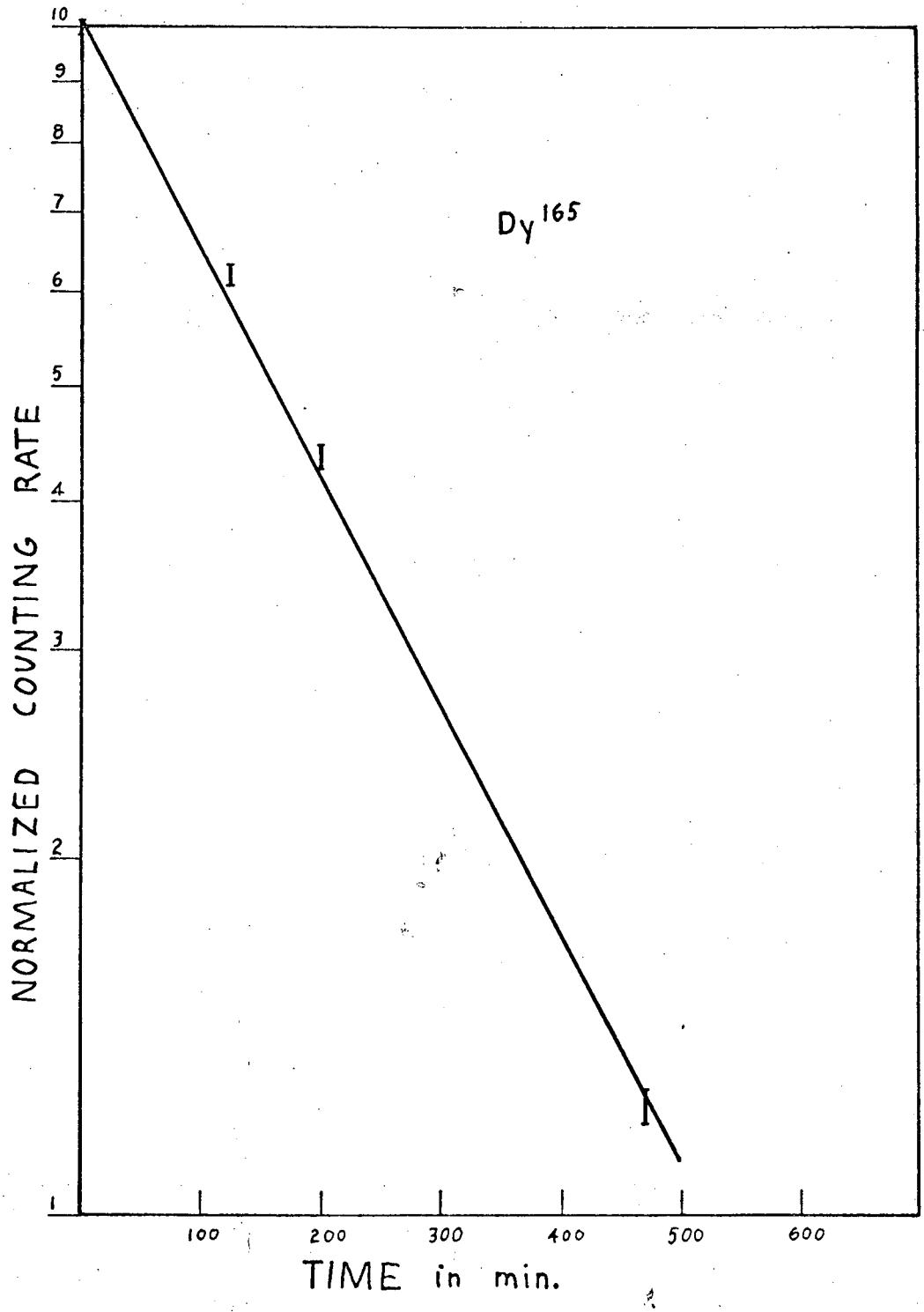

Fig. VI-1. Decay of Dy^{165}.

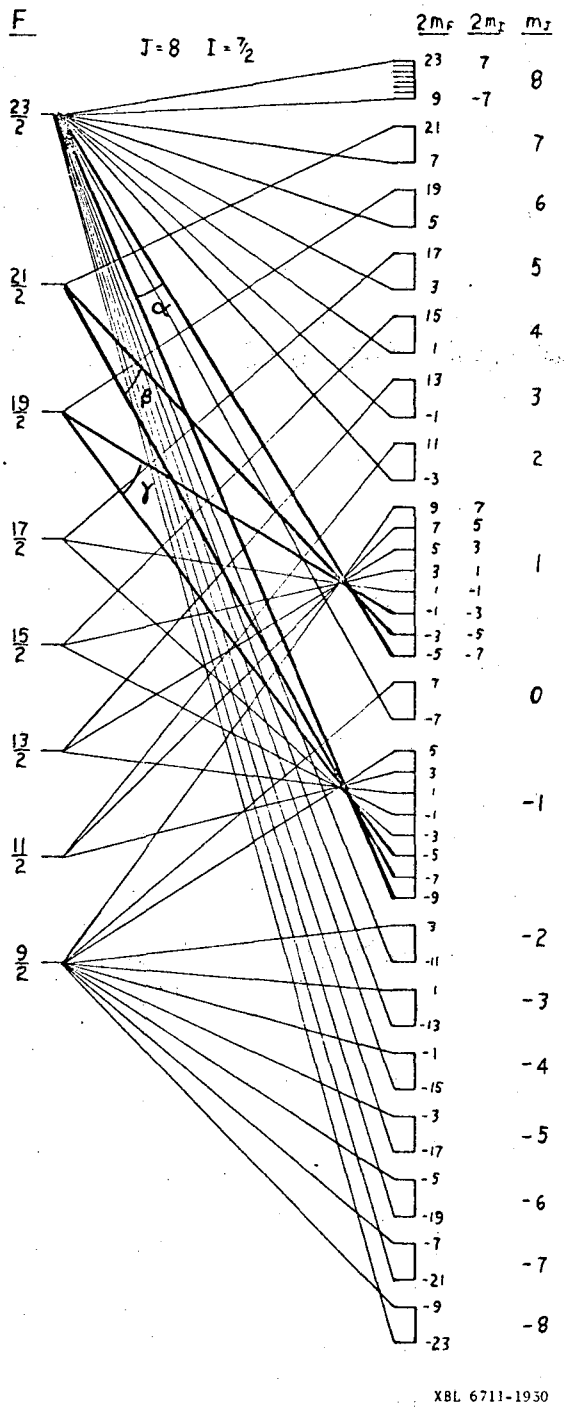

Fig. VI-2. Hyperfine structure diagram (partial schematic) for Dy^{165}.

F = 23/2 state, with sufficient r.f. power, one might induce up to eight transitions, from $m_F = 1 \leftrightarrow -1$ to $m_F = 8 \leftrightarrow -8$, but for the lowest state, F = 9/2, there is only one refocusable transition, $m_F = 1 \leftrightarrow -1$.

The hyperfine structure was investigated by studying the magnetic field dependence of the three highest F transitions. Resonances were first traced out in the low field region where their frequencies are reliably predicted by Eq. (3.22). They were then followed to higher fields by using first linear and then quadratic extrapolation. When appreciable deviation from linearity had been observed, attempts were made to fit values of the parameters a and b to the field-vs.-frequency data by using the computer routine "Hyperfine 4" (ZUR 64). The values of a and b thus obtained were then fed into computer routine "Hyperfine 2" (SHU 66) to predict the proper transition frequencies for higher fields.

In the case of Dy^{165} the shifts from the a=b=0 lines for the three highest F levels occurs at moderately low fields and it was only necessary to go up to fields of 220 gauss to obtain a to better than one percent. As a rule of thumb one can use Eq. (6.1) to predict the accuracy of a if there is no correlation between a and b .

$$\frac{1}{\text{Accuracy of } a} \approx \sqrt{\sum_{\substack{\text{each resonance} \\ \text{at each field}}} \left(\frac{\text{deviation from a=b=0 line}}{\text{accuracy of resonance}} \right)^2} \qquad (6.1)$$

2. Results

Ten resonances were used to give reasonably good values of a and b . As seen from Table VI-I, four α, and four β, and two γ transitions in fields ranging from 30 to 220 gauss constitute the data. All transitions

Table IV-1. Dysprosium-165 Resonances

H(G)	ν_{exp}(MHz)*	Residual	Transition	Deviation from a=b=0 line (MHz)*
30.00(5)	73.00(16)	-0.21	α	+0.46(16)
30.00(5)	76.60(16)	-0.18	β	+0.16(16)
50.00(5)	122.80(16)	-0.02	α	+1.90(16)
50.00(5)	128.54(16)	0.16	β	+1.12(16)
50.00(5)	136.80(16)	0.19	γ	+0.90(16)
100.00(5)	249.60(24)	-0.19	α	+7.80(24)
100.00(5)	258.90(20)	-0.24	β	+4.10(20)
100.00(5)	274.90(20)	-0.16	γ	+3.10(20)
220.00(5)	571.76(20)	0.03	α	+39.80(20)
220.00(5)	586.20(50)	0.25	β	+25.64(50)

a(MHz)	Δa	b(MHz)	Δb	g_J	χ^2
±89.83	0.65	∓1520	28	-1.24166	5.4

Residual = $\nu_{exp} - \nu_{theo}$

Transition α F = 23/2 $m_F = -5/2 \leftrightarrow -9/2$

β F = 21/2 $m_F = -3/2 \leftrightarrow -7/2$

γ F = 19/2 $m_F = -1/2 \leftrightarrow -5/2$

*Frequencies are twice the actual applied frequency since J being integral leads to a two quantum transition.

are $\Delta F = 0$, and an α transition is one involving F_{max}, a β transition (F_{max}-1) and a γ transition (F_{max}-2) as shown in Fig. VI-2.

As can be seen from Fig. VI-3 there is no question as to the assignment of levels and since b/a = -16.9 is very far from a level ordering crossing as shown in Fig. VI-4 there is no possibility of a direct transition being misinterpreted as a $\Delta F = 0$ transition. The closest zero-field level order crossings occur at b/a = -37.3 and b/a = +29.5 (BAK 60).

It should be noted that the frequencies and deviations listed in Table VI-1 are double those used experimentally since one is dealing with double quantum transitions.

The final results are

$$a = \pm 89.8(7) \text{ MHz} \qquad I = 7/2$$
$$b = \mp 1520(30) \text{ MHz}$$
$$b/a = -16.9$$

Penselin's values for Dy^{161} are (PEN 64)

$$a = -115.8\ (10) \qquad I = 5/2$$
$$b = +1102(15)$$
$$\mu_I = -0.46(19)$$
$$Q = 2.02(40)$$

Using the Fermi-Segrè relations [Eqs. (3.9) and (3.14)] with Dy^{161} one obtains for Dy^{165}

$$\mu_I(\text{uncorr}) = \mp 0.50(4) \text{ nm}$$
$$Q(\text{uncorr}) = \pm 2.8(3) \text{ barns}$$

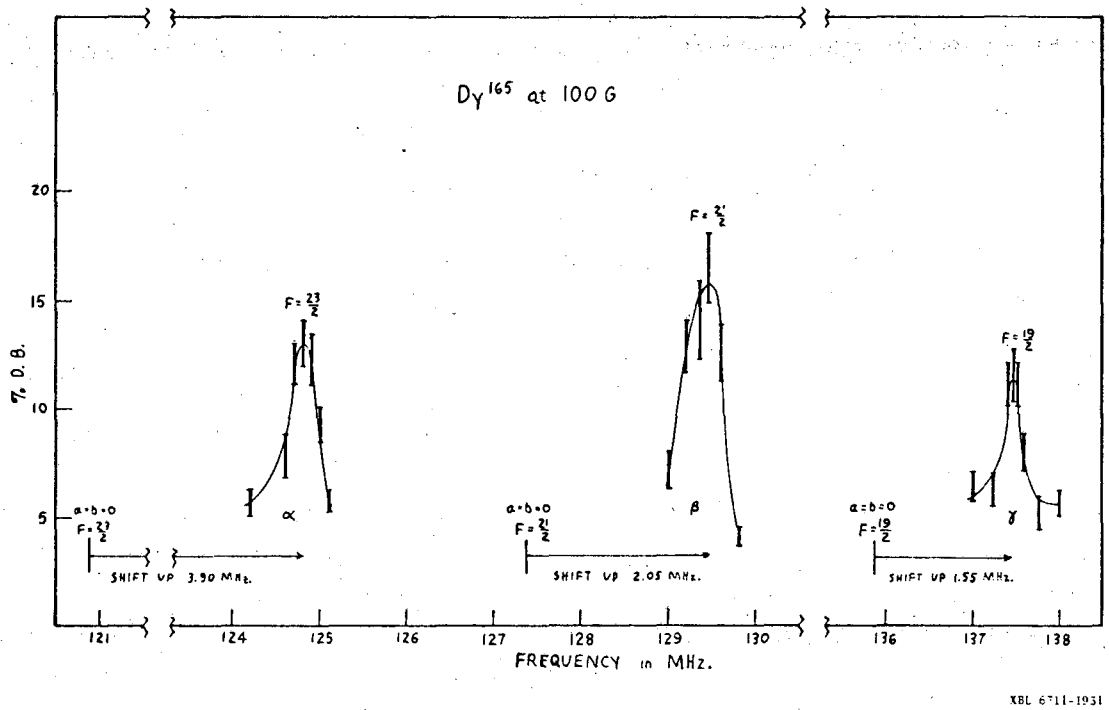

Fig. VI-3. α, β and γ transitions for Dy^{165} at 100 gauss.

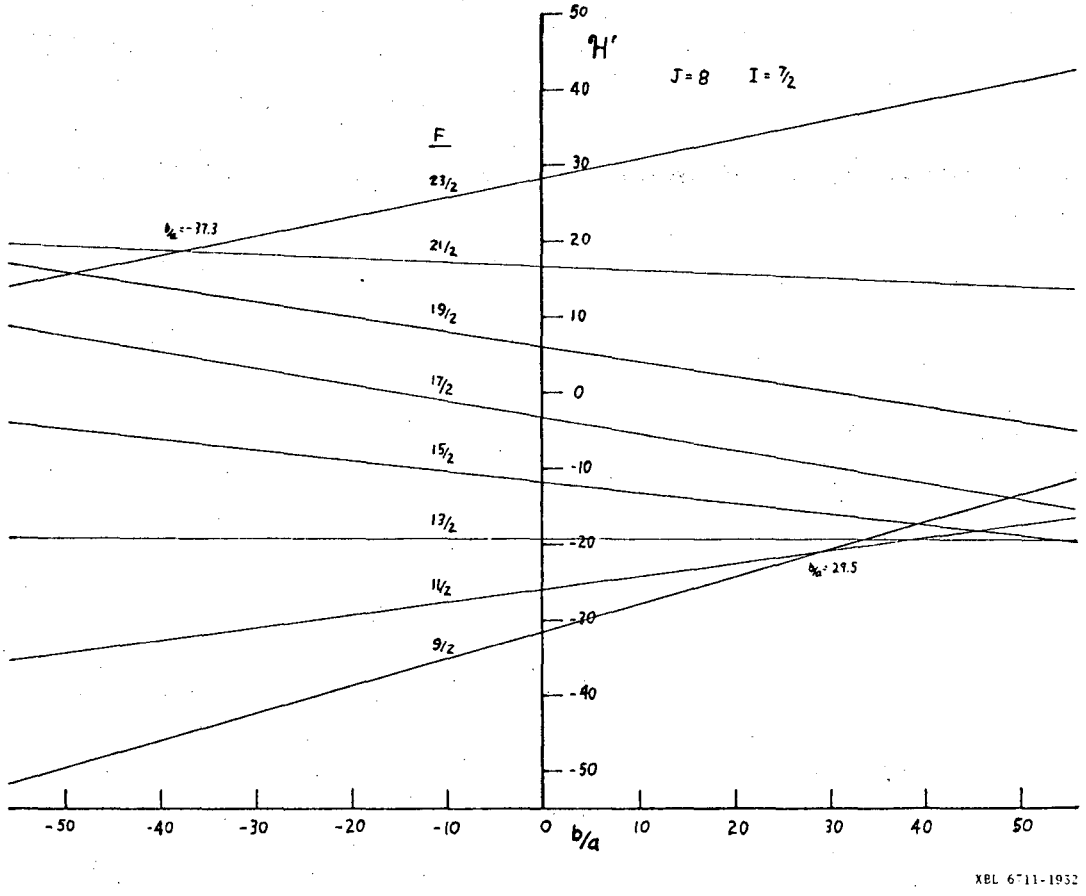

Fig. VI-4. Zero field level ordering for Dy^{165}.

Using Eqs. (3.7) and (3.8) for μ_I and Eqs. (3.12) and (3.13) for Q and Bleaney's value for $\langle\frac{1}{r^3}\rangle$ (BLE 64) which is $\langle\frac{1}{r^3}\rangle$ = 8.7 a.u. one obtains for Dy^{165}

$$\mu_I(\text{uncorr}) = -0.50(4) \text{ nm}$$
$$Q(\text{uncorr}) = 2.8(3) \text{ barns}$$

where the sign of Q has been chosen positive since most isotopes in this region (150<A<190) have positive quadrupole moments, thus fixing the sign of μ_I. No diamagnetic or Sternheimer corrections have been applied.

3. Interpretation

Dy^{165} has 66 protons and 99 neutrons in its nucleus. It is thus far removed from closed shells (50, 82, 126) which places it in a strongly deformed region. The collective model of Nilsson (NIL 55) applies in this region. The ground state of Dy^{165} is characterized by the asymtotic Nilsson orbital of 7/2 + [633] (MOT 59) for the 99^{th} neutron. Fig. IV-2 "is apparently in error in predicting the [521-1/2] level to be below the [633-7/2] level. In every case where clear cut experimental evidence is available, the latter level is found to lie somewhat below the former." (Direct quote from (MOT 59)).

From Eqs. (4.2) and (4.3) and Q = 2.8 barns one obtains δ = 0.24. A systematic study of Chiao (CHI 61) of the magnetic properties of deformed nuclei indicates that in the region of A = 165, the deformation δ is a slowly varying parameter and is approximately equal to 0.26. Using δ = 0.26 one gets Q = 3.2 barns, about 14 % above the value calculated from the measured interaction constant b .

From Eq. (4.1) with $g_R = Z/A$, $g_\delta(n) = -3.826$ and $g_\ell(n) = 0$ for $\delta = 0.3$ one obtains $\mu_{calc} = -0.80$ which is 60% above the value obtained from a . A value of g_δ less than the free value would bring μ_{calc} into better agreement. For $g_\delta(n) = -2.9$ one gets $\mu_{calc} = -0.50$ which is the measured value. By interpolating the $a_{\ell,\Omega}$'s to $\delta = 0.26$ and using $g_\delta(n) = -2.4$, $g_R = \frac{Z}{2A} = 0.20$ as recommended by Chiao, one obtains $\mu_{calc} = -0.51$ compared with $\mu_{meas} = -0.50$.

The agreement between the calculated values of μ (using a quenched g_δ) and Q and the values deduced from a and b is very good, considering the uncertainties in the atomic calculations. The results again confirm the applicability of the Nilsson individual-nucleon, strong-deformation approach in this region of the periodic table.

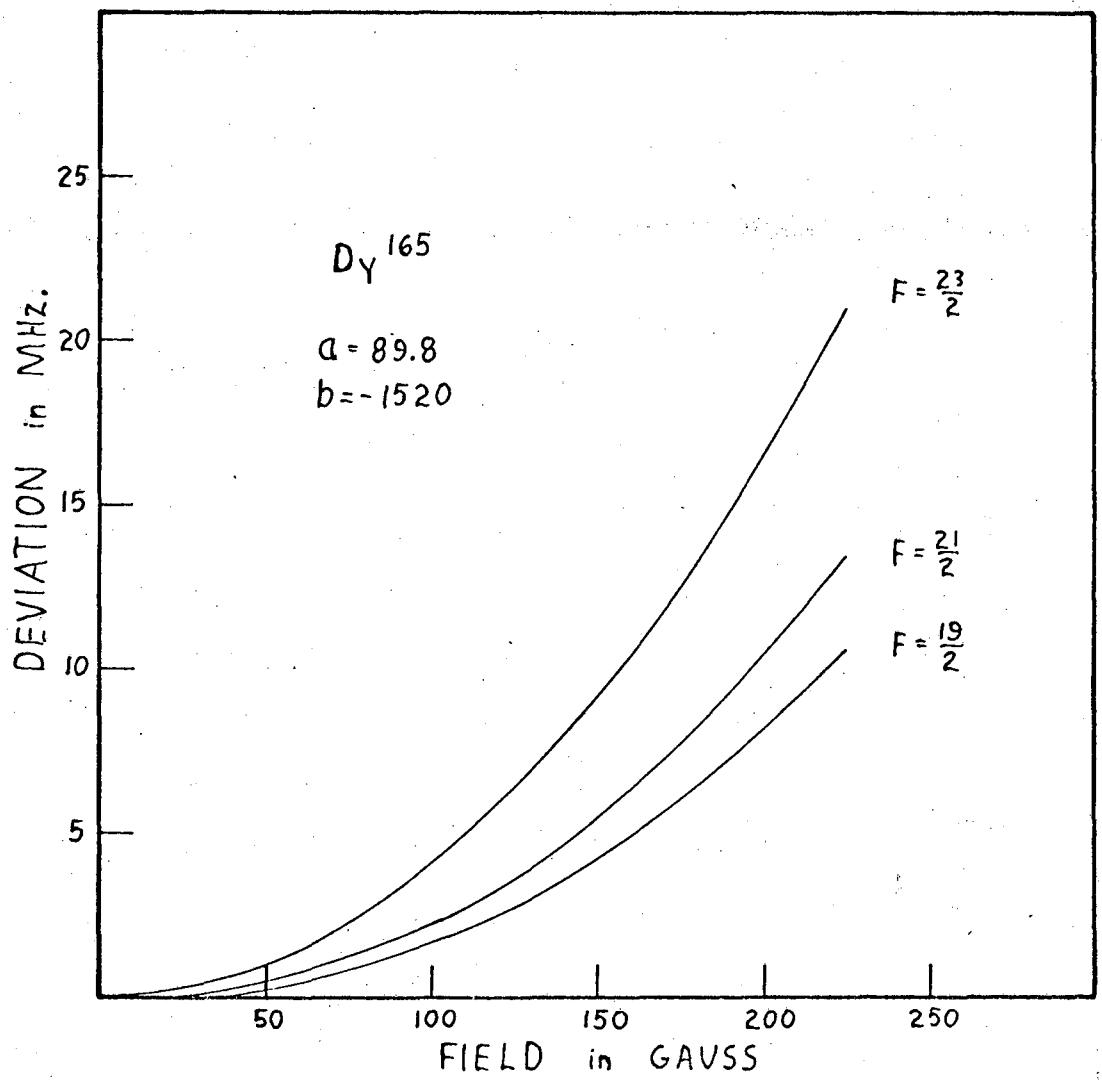

XBL 6711-1933

Fig. VI-5. Deviations from a=b=0 lines for Dy^{165} for F = 23/2, 21/2 and 19/2.

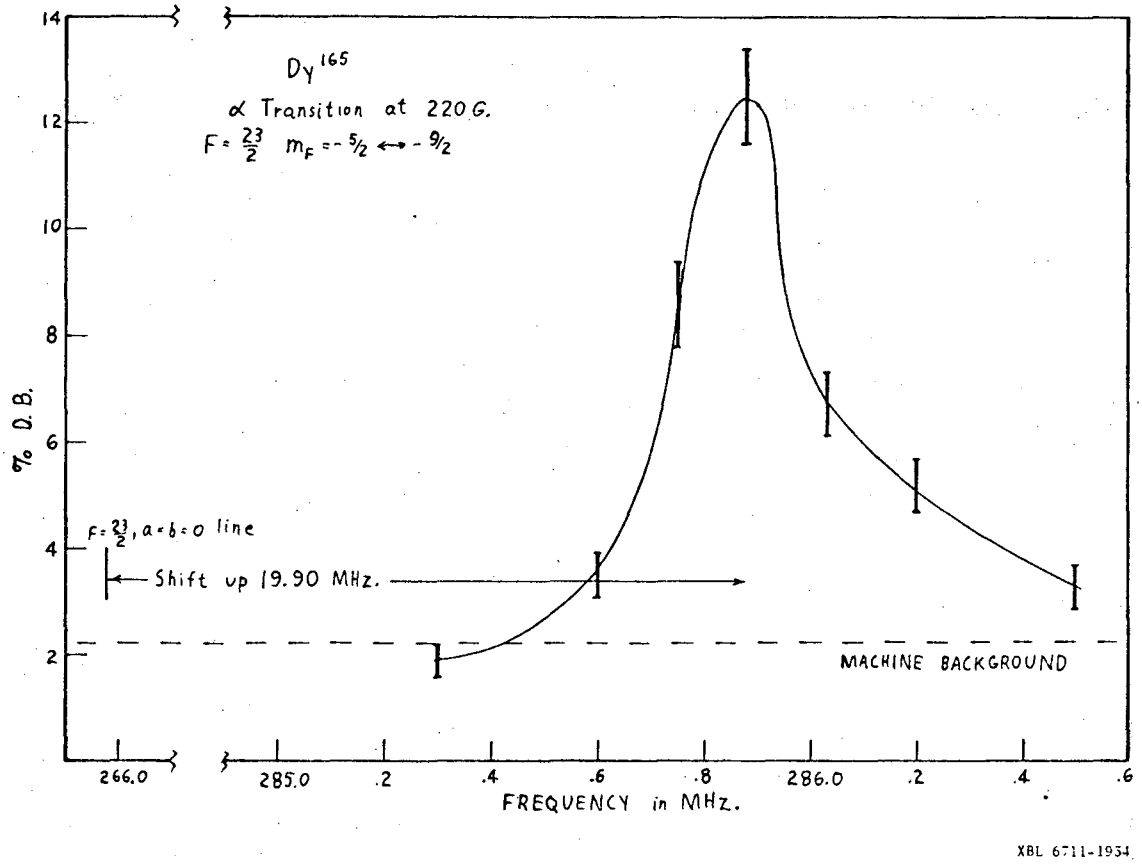

Fig. VI-6. α transition for Dy^{165} at 220 gauss.

B. Spin of Erbium-163

1. Introduction

Er^{163} has a half-life of 75 minutes, decaying by β^+ emission to Ho^{163} (half-life > 10^3 years), then by electron capture to stable Dy^{163}. Er^{163} was made by bombarding stable Ho^{165} (100% abundant) on the 88-inch Cyclotron at Berkeley with 37 Mev protons for about two hours at a current of 30 μamps or greater producing the reaction Ho (p,3n) Er^{163}. As is evident from Fig. VI-7 only Er^{163} was produced in detectable amounts. The decay curve is a straight line for 6 hours (∿ 4.5 half-lifes).

The cyclotron target as shown in Fig. VI-8 consists of four disks, 0.230" in diameter and 0.050" thick, and a 5 mil cover foil of aluminum. The disks were placed in a Ta or W oven and oven liner and heated by electron bombardment until a satisfactory beam was obtained. About 100 watts of heating was necessary. The beam lasted about four hours. Sometimes the sample melted and evaporated out of the oven, other times the sample looked as if nothing had happened to it. Anywhere from 1/2 to 2 hours was occupied trying to get a satisfactory beam. The erbium didn't necessarily come out as single atoms at first. Heating the sample to a higher temperature initially and then lowering the temperature seemed to help in getting an atomic beam. One could not start taking data until one obtained a previously seen resonance. A temperature giving a direct beam in excess of a hundred counts per minute was a satisfactory temperature to work at. Er^{169} was used to determine g_J to high accuracy, g_J = -1.16381(5) (DOY 63).

2. Spin Search

Erbium has a $^3H_6$ ground state arising from $4f^{12}6s^2$ configuration. Er^{163} has 68 protons and 95 neutrons for a total of 163 nucleons which

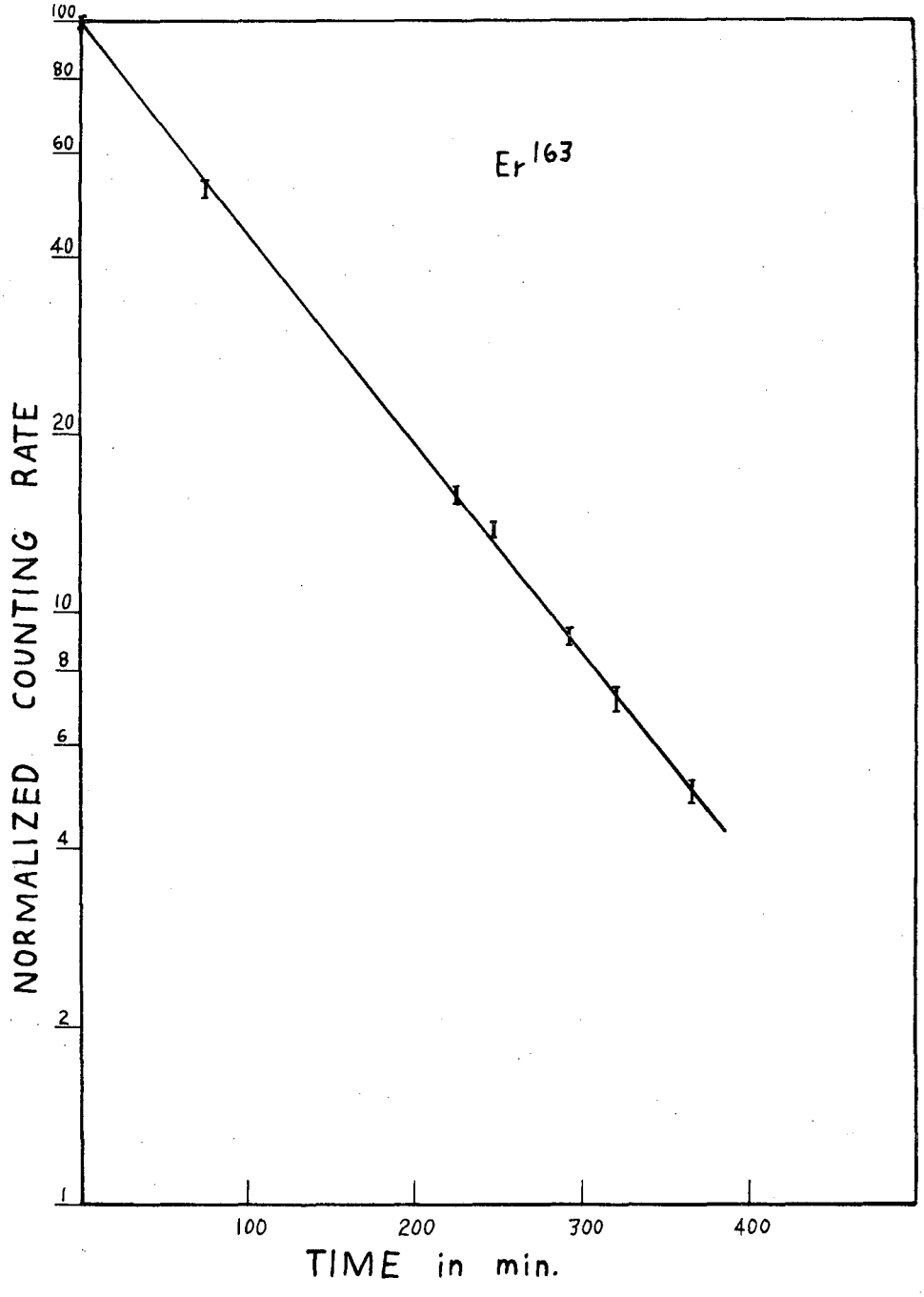

XBL 6711-1935

Fig. VI-7. Decay of Er^{163}.

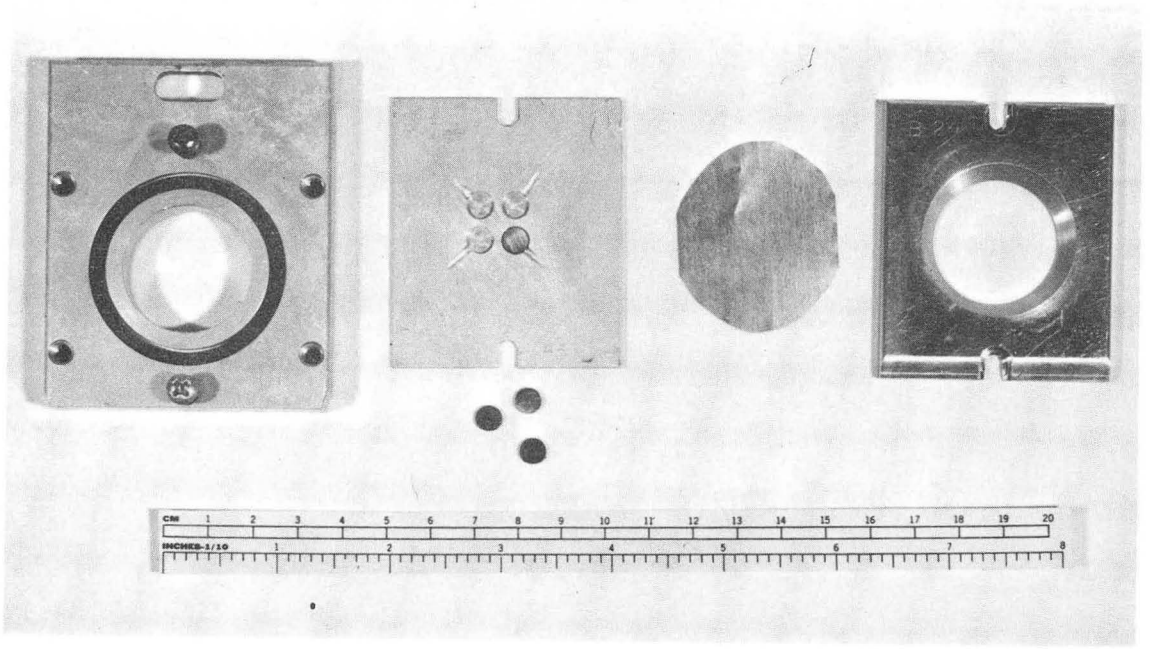

XBB 6711-6663

Fig. VI-8. Cyclotron target and Ho disks.

gives rise to a half integral spin. Spins from I = 1/2 to I = 11/2 were tried using Eq. (3.22) at four and six gauss as shown in Figs. VI-9 and VI-10. The spin was found to be I = 5/2. From Fig. VI-10, the six gauss spin search, it is obvious that something unusual is happening since the F = 17/2 and F = 15/2 points have decreased by more than 50% from those of Fig. VI-9 taken as four gauss. This can be explained by looking at Fig. VI-II where the resonances at six gauss are shown. The resonances have appreciable shift at as low a field as six gauss. At 12 gauss, Fig. VI-12, one can see only one resonance. Another point to be noted is the decrease in amplitude in going from six gauss (76%) to 12 gauss (44%).

With a spin of 5/2 there are 78 Zeeman sublevels in the beam, giving rise to six Zeeman flop-in resonances as shown in Fig. VI-13. Five of the six transitions yielded large resonances at 10 gauss (>25%) while the sixth (F = 7/2) was much smaller.

3. Interpretation

Since Er^{163} is far removed from a closed shell, it is in a strongly deformed region. The collective model of Nilsson applies in this region. The ground state of Er^{163} is characterized by the asymtotic Nilsson orbital of 5/2-[523] (MOT 59) for the 95^{th} neutron. The measured spin I = 5/2, agrees with that predicted by the Nilsson model, Fig. IV-2.

4. Higher Field Results

The three highest F states were traced out at higher fields. At 20 gauss, the F = 17/2 and F = 15/2 transitions have separated into two distinct resonances as shown in Fig. VI-14, but there was a problem in assigning F values to the resonances. Whichever one the F = 17/2 resonance is, it was shifted up from the a=b=0 line and the F = 15/2

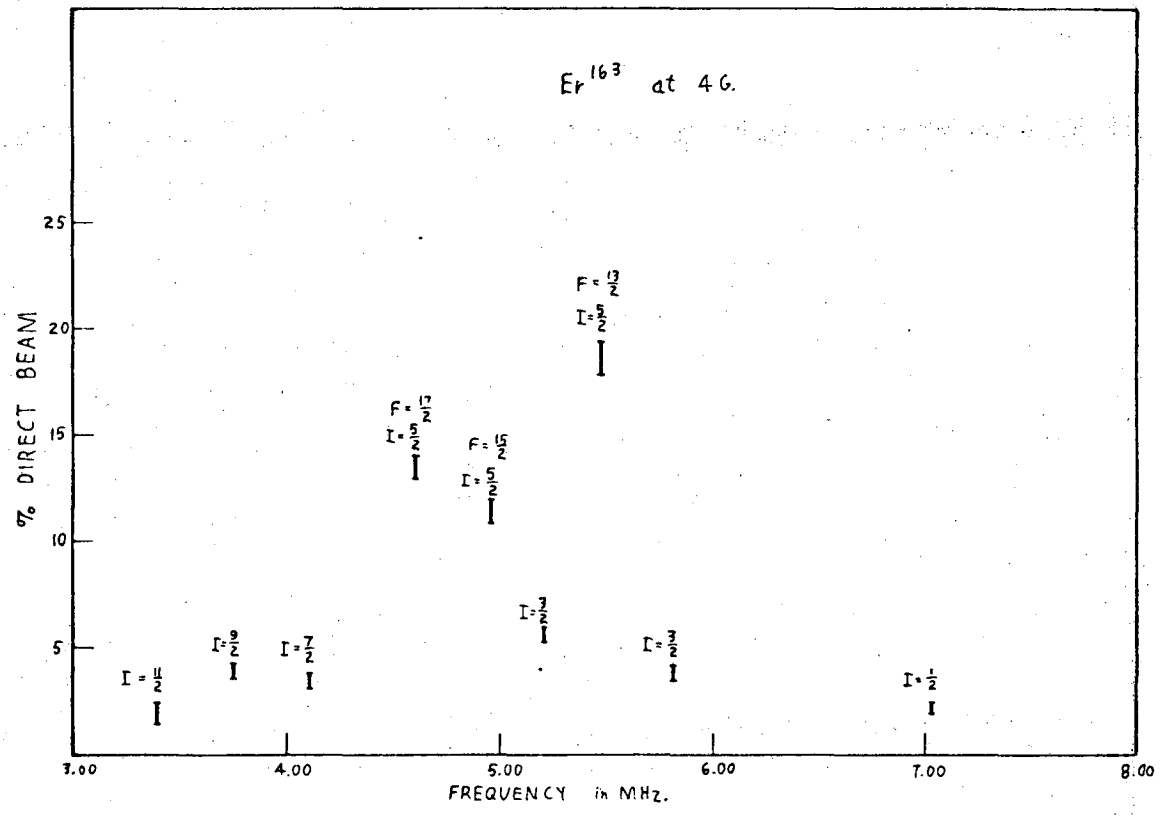

Fig. VI-9. Er^{163} spin search at 4 gauss.

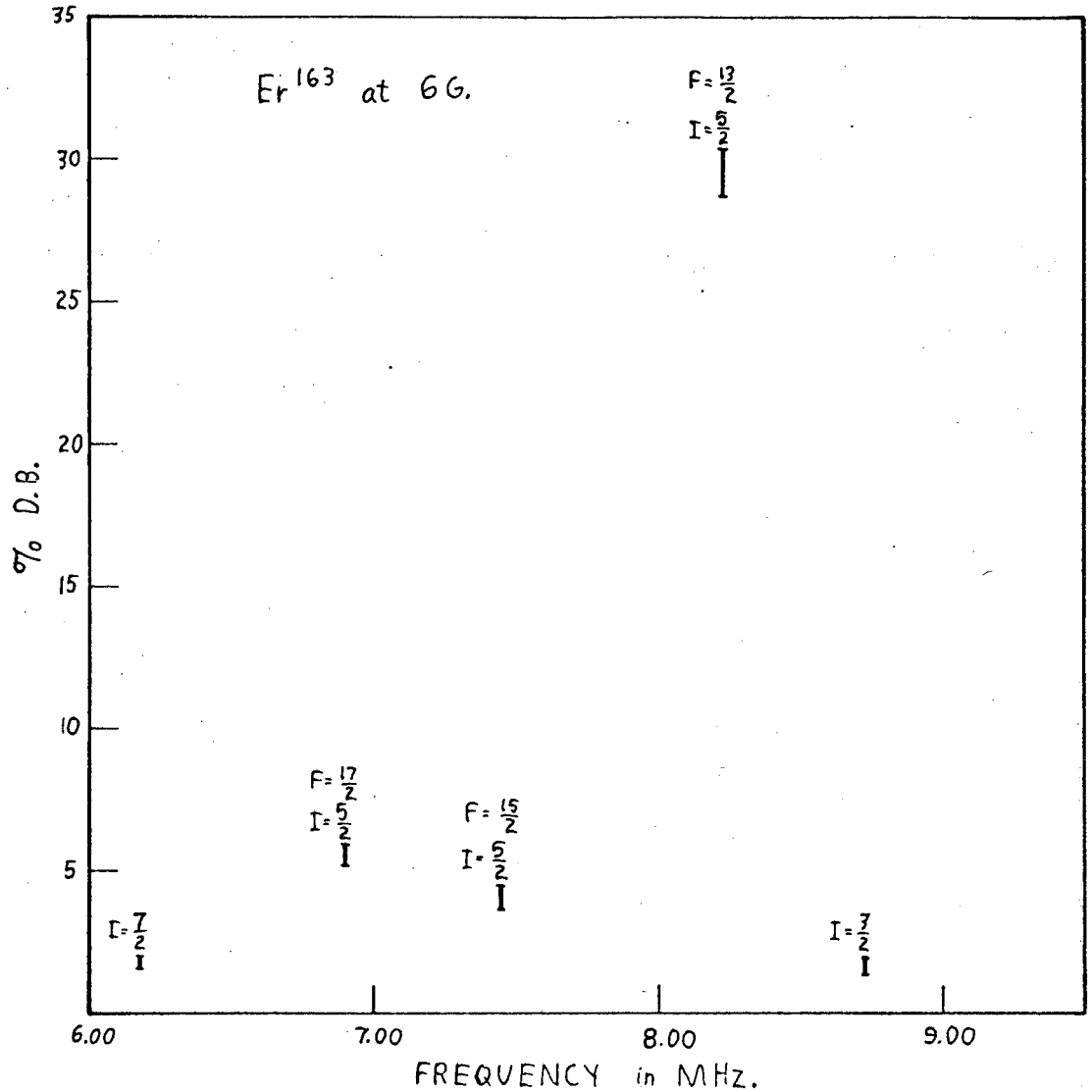

Fig. VI-10. Er^{163} spin search at 6 gauss.

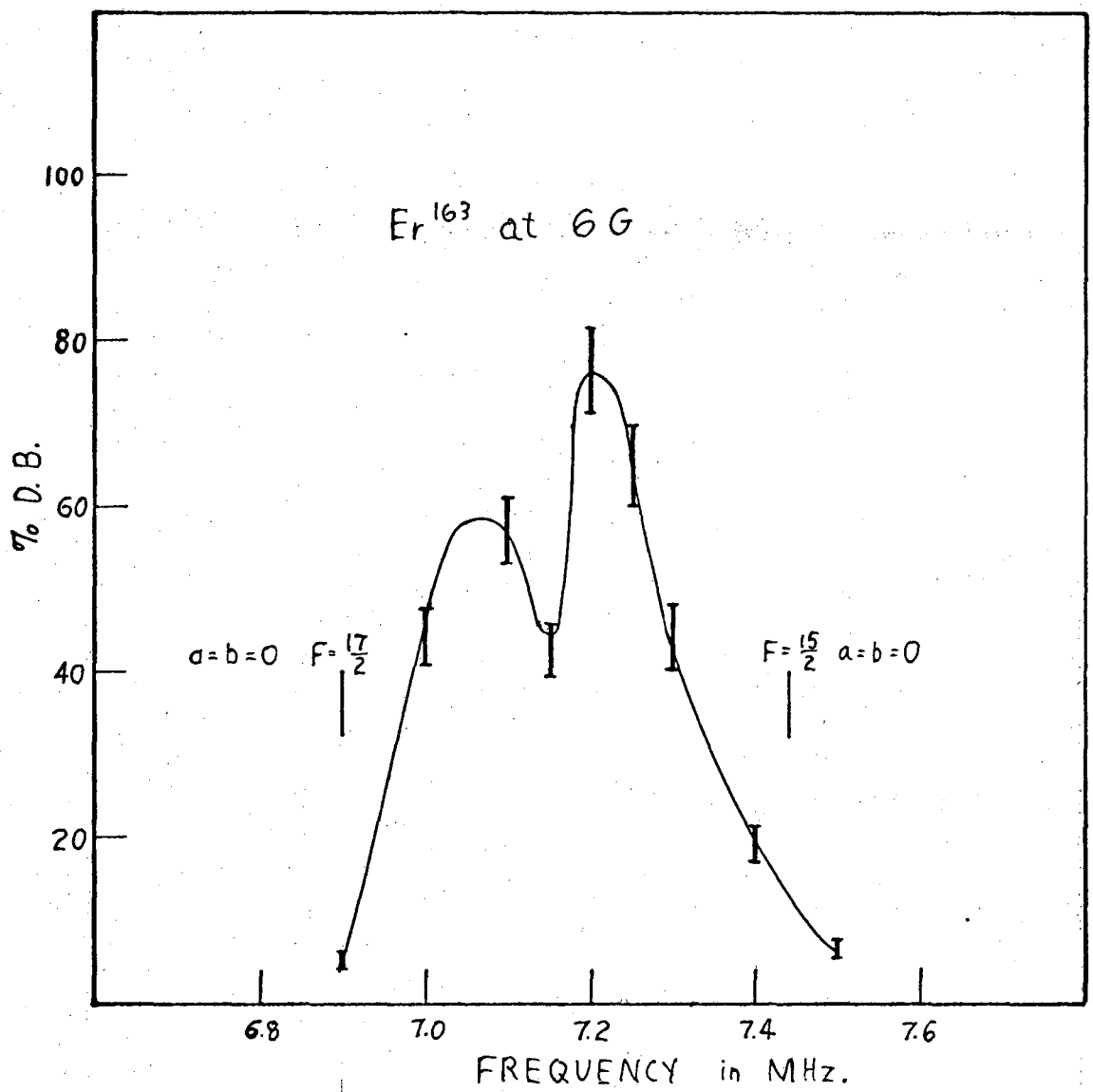

XBL 6711-1938

Fig. VI-11. Er^{163} resonance at 6 gauss.

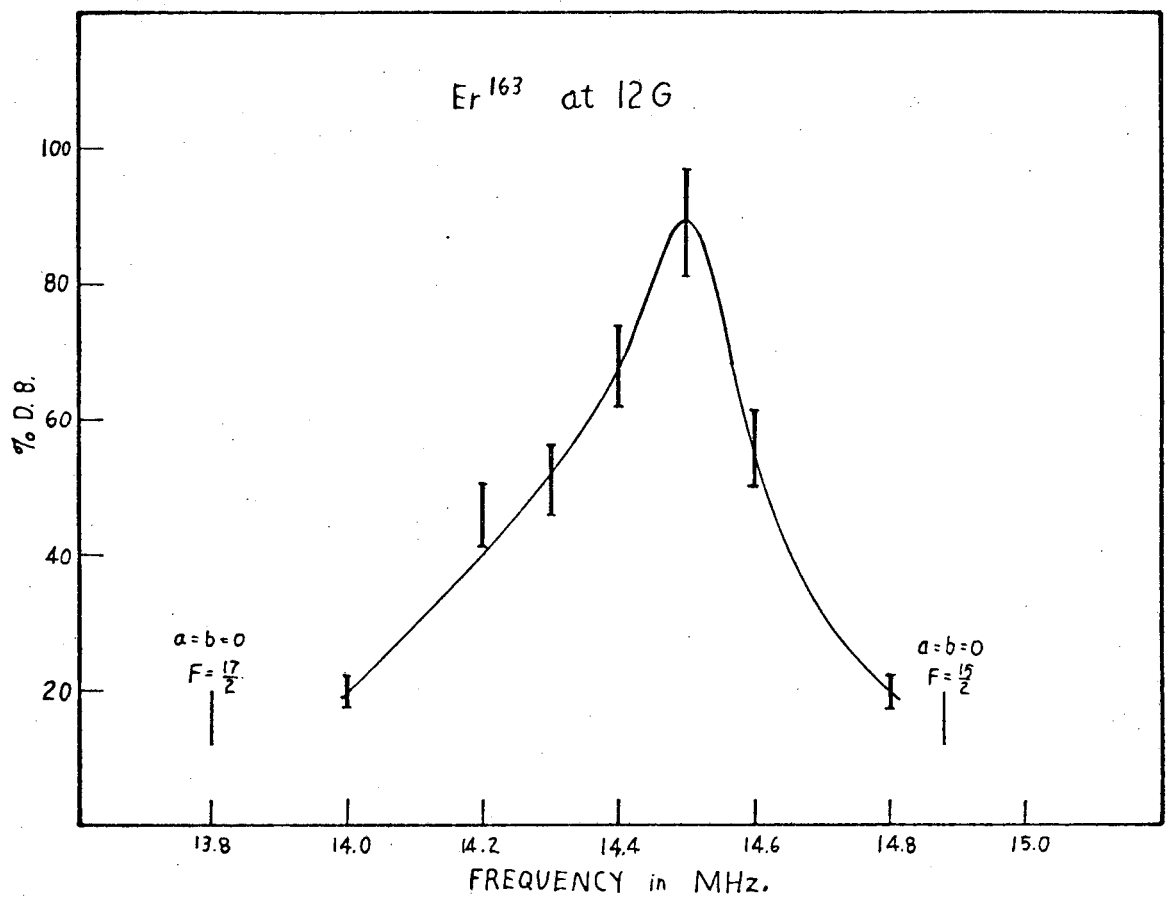

XBL 6711-1939

Fig. VI-12. Er^{163} resonance at 12 gauss.

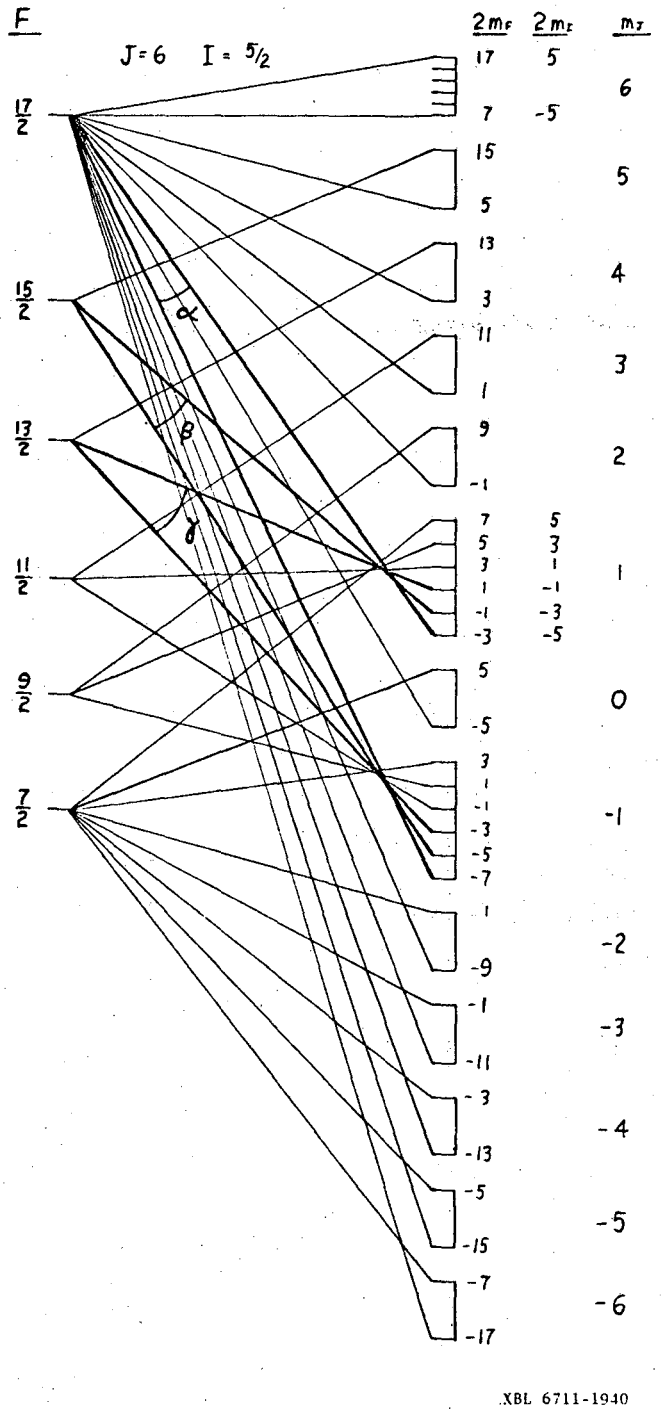

Fig. VI-13. Hyperfine structure diagram (partial schematic) for Er^{163}.

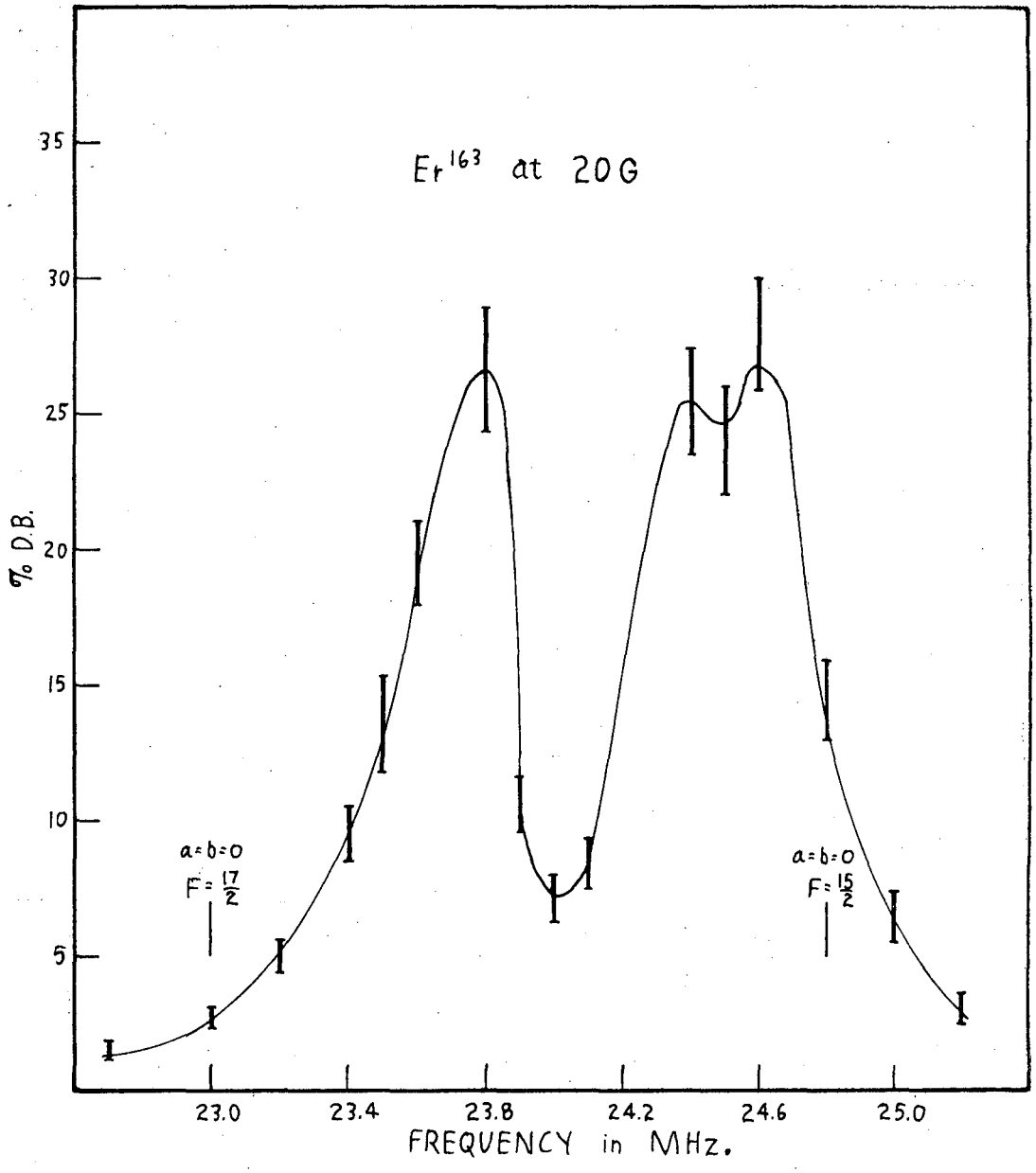

XBL 6711-1941

Fig. VI-14. Er^{163} resonance at 20 gauss.

resonance was shifted down as can be seen from Fig. VI-14. With this in mind "Hyperfine 2" was run for a values from 100 to 400 and b values from +9000 to -10,000 for both F = 17/2 and F = 15/2. The F = 13/2 resonance was not shifted at 20 gauss. The results of the computer run are shown in Figs. VI-15 and VI-16 where deviations from the a=b=0 lines are plotted at 20 gauss for F = 17/2 and F = 15/2. The only region of the plots where one gets the proper deviations is near the b/a = -20.0 line. As can be seen from Fig. VI-17 the F = 17/2 and F = 15/2 lines cross at b/a = -20.0 at zero field (BAK 60).

Figure VI-18 is a plot of the deviations with magnetic field from the a=b=0 line for F = 15/2 for a from 100 to 400 and b/a from -10 to -19.5. The deviations all tend away from the a=b=0 line and there is no tendency for the lines to cross the a=b=0 line other than at zero field. Figure VI-19 is a plot of the a=b=0 lines for F = 17/2 and F = 15/2 with the experimental data superimposed. There are two possible ways to connect up the experimental points. The dotted line for F = 15/2 tends toward the a=b=0 line at higher fields. This can't be correct since all F = 15/2 curves as shown in Fig. VI-18 tend away from the a=b=0 line. Therefore the solid lines in Fig. VI-19 are the correct ones. This is born out by higher field data. The F = 17/2 line crosses the a=b=0 line for F = 15/2 at about 50 gauss.

Seven resonances were used to obtain values of a and b . As shown in Table VI-2, three α, two β and two γ transitions in fields ranging from 20 to 130 gauss constitute the data. The intensity of the resonances decreased as one went to higher fields. At 130 gauss the F = 17/2 resonance as shown in Fig. VI-20 is 6.4% and the F = 15/2 resonance

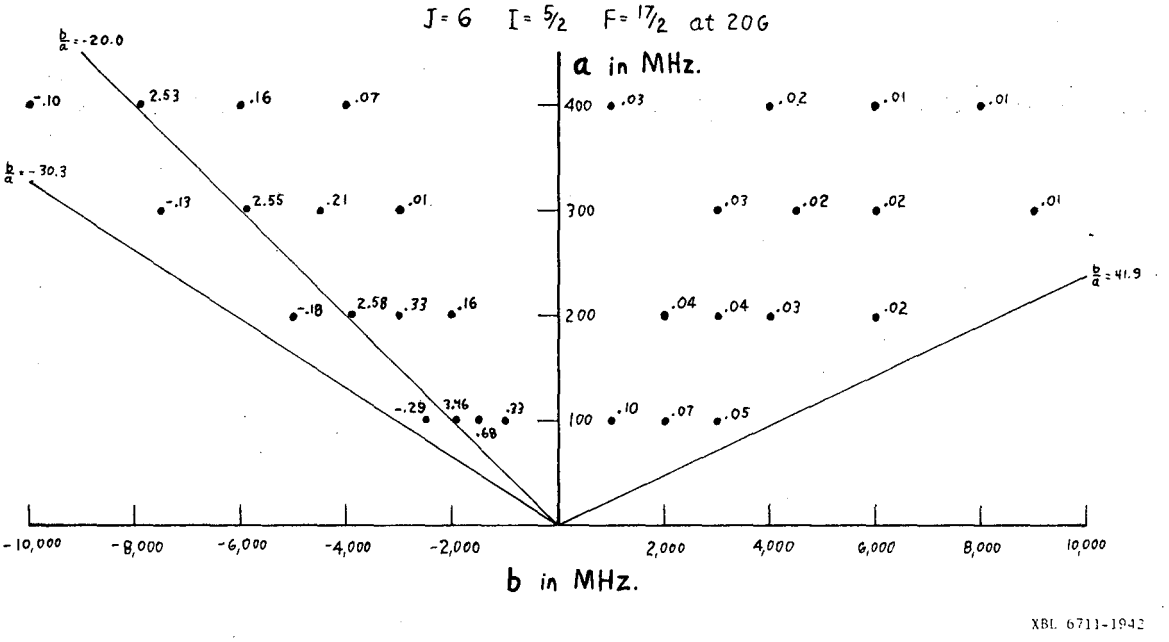

Fig. VI-15. Deviations from a=b=0 line for various a's and b's at 20 gauss for F = 17/2.

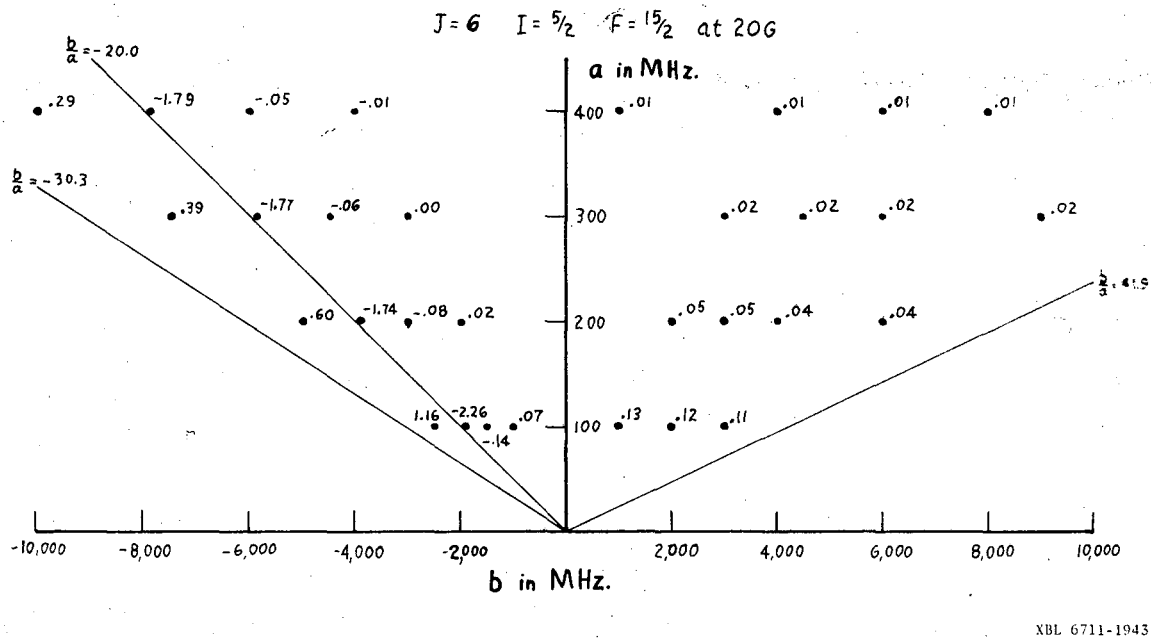

Fig. VI-16. Deviations from a=b=0 line for various a's and b's at 20 gauss for F = 15/2.

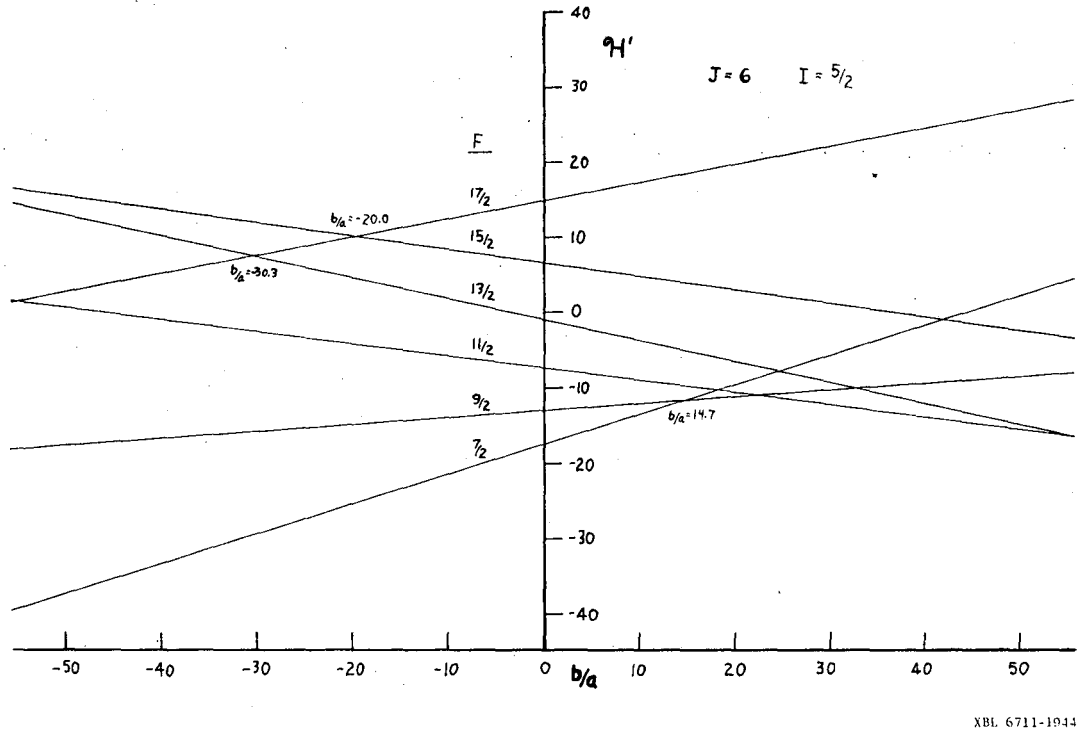

Fig. VI-17. Zero field level ordering for Er^{163}.

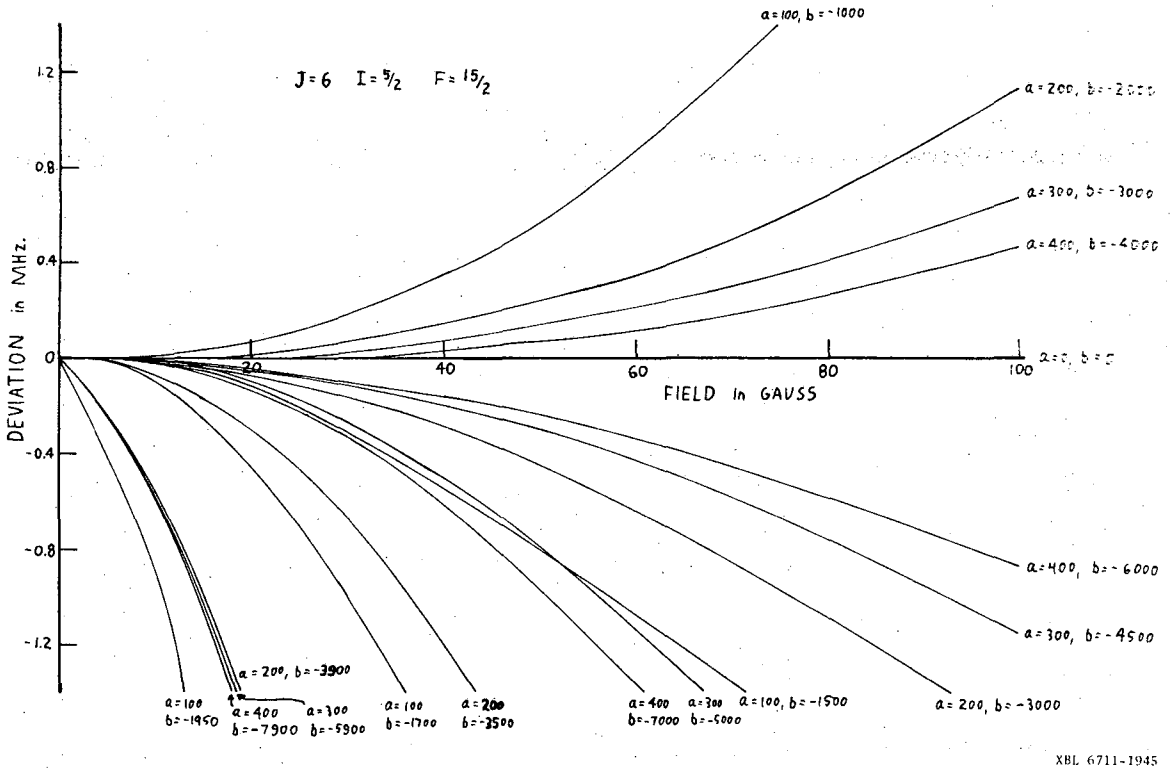

Fig. VI-18. Deviations from a=b=0 line for various a's and b's for F = 15/2.

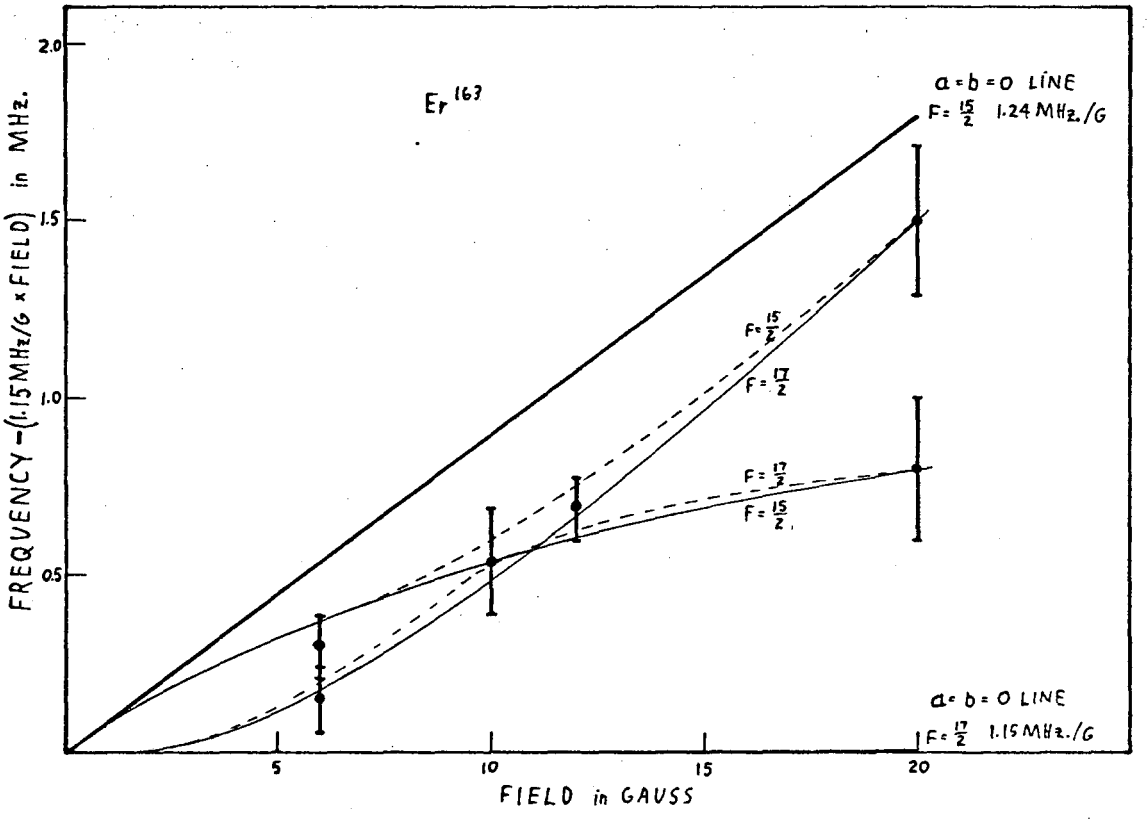

Fig. VI-19. Resonances for Er^{163} to 20 gauss for F = 17/2 and 15/2 (amplified scale).

Table VI-2. Erbium-163 Resonances

H(G)	ν_{exp}(MHz)*	Residual	Transition	Deviation from a=b=0 line (MHz)*
20.00(5)	49.00(30)	-0.07	α	+3.00(30)
20.00(5)	47.40(30)	0.00	β	-1.80(30)
20.00(5)	54.80(40)	0.00	γ	0.00(40)
50.00(5)	124.80(40)	0.25	α	+9.80(40)
50.00(5)	137.20(40)	0.20	γ	0.00(40)
130.00(5)	328.20(20)	-0.02	α	+29.20(20)
130.00(5)	305.20(30)	0.04	β	-17.20(30)

a(MHz)	Δa	b(MHz)	Δb	g_J	χ^2
±314.0	12.5	∓6220	252	-1.16381	0.6

Residual = $\nu_{exp} - \nu_{theo}$

Transition α F = 17/2 $m_F = -3/2 \leftrightarrow -7/2$

β F = 15/2 $m_F = -1/2 \leftrightarrow -5/2$

γ F = 13/2 $m_F = +1/2 \leftrightarrow -3/2$

*Frequencies are twice the actual applied frequency since J being integral leads to a two quantum transition.

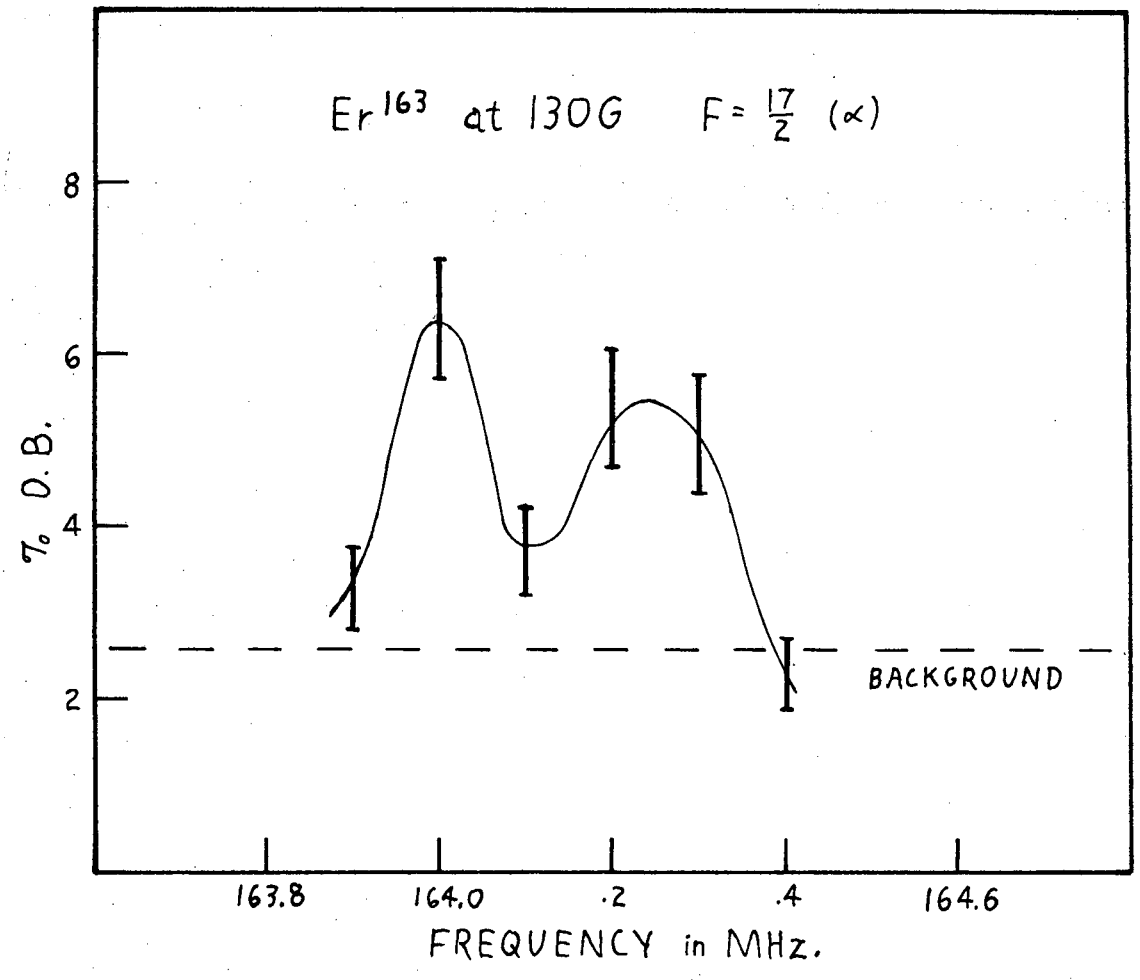

XBL 6711-1947

Fig. VI-20. α transitions for Er^{163} at 130 gauss.

is only 1.7%. Both resonances have a pronounced dip in the middle. The dip could be due to r.f. overdriving. The decrease in amplitude with increase in frequency is most likely due to the shift in frequencies for the individual single quantum transitions that make up the double quantum transition.

Since b/a = -19.80 is very close to a level ordering crossing there could be a possibility of a direct transition being misinterpreted as a $\Delta F = 0$ transition. The normal direct transition $\Delta F = 1$, $\Delta m_F = \pm 1$ (π transition) which is theoretically refocusable is labeled I in Fig. VI-21. II and III are σ transitions that are not theoretically refocusable but if the oven hole is off center and the beam goes by the edge of the hairpin in the "C" region there is a possibility of their being refocused. "Hyperfine 2" was used to compute these three transitions for a from 100 to 400 and b/a near -20. The three transitions plotted in Fig. VI-21 are for $a = 314$ and $b = -6220$ since all the direct transitions from $a = 100$ to 400 for various b/a's are similar. As can be seen from the figure there is no possibility of the direct transitions being misinterpreted as a $\Delta F = 0$ transition.

For $a = 314$ and $b = -6220$ at 250 gauss one gets from "Hyperfine 2" a deviation of -0.7 MHz for F = 13/2, -0.2 MHz for F = 11/2, -1.0 MHz for F = 9/2 so there was no point in obtaining resonances for these F values unless one used a much higher magnetic field. For F = 17/2 and F = 15/2 the intensity was low at 130 gauss so a possible way to get more accurate values for a and b would be to use two distinct frequencies for the double quantum transitions. The deviations for F = 17/2 and F = 15/2 at 130 gauss should have been enough to determine a to better than 1% had a and b not been correlated. If Eq. (6.2)

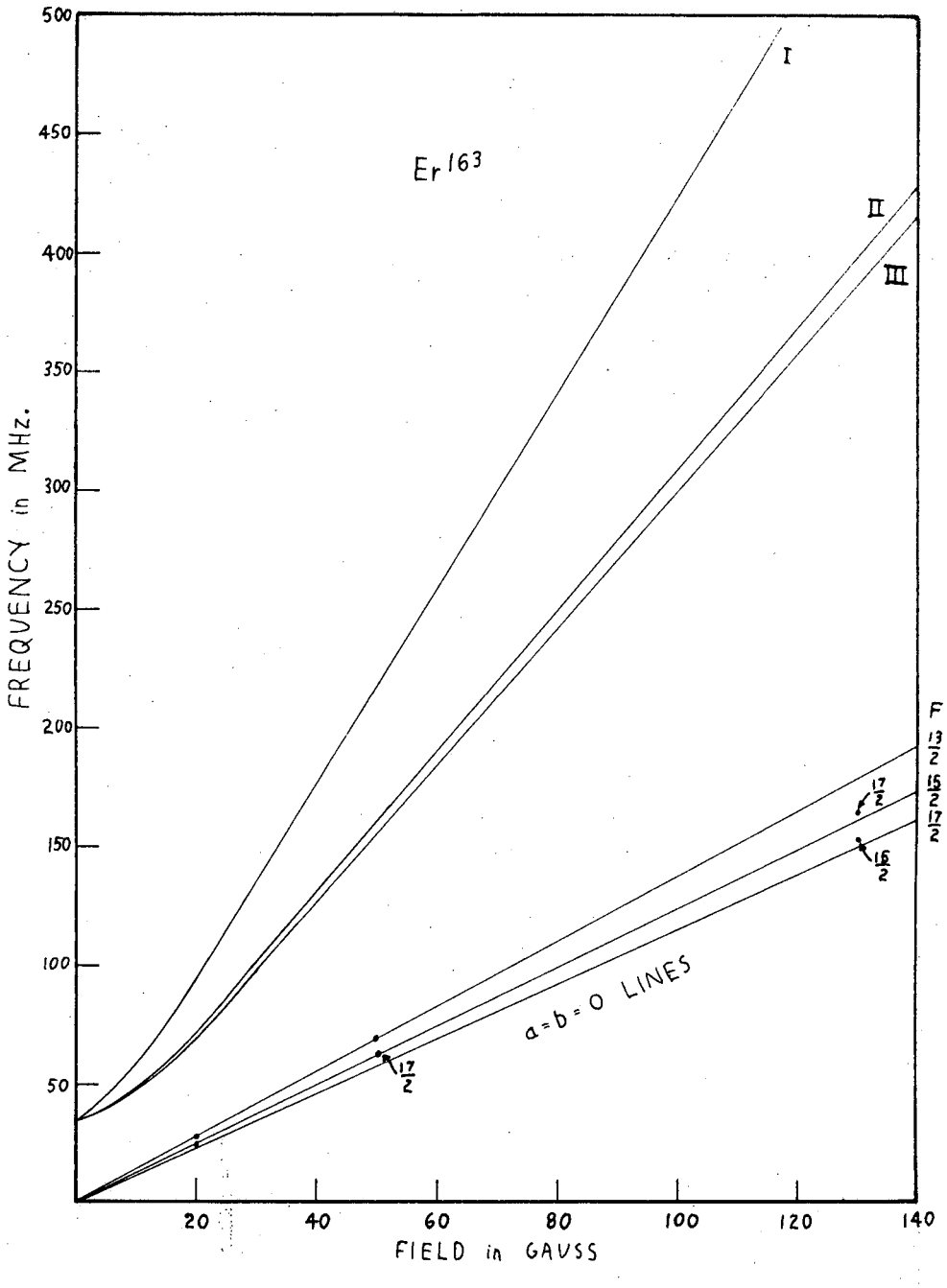

XBL 6711-1948

Direct Transitions

I $F = 17/2,\ m_F = -3/2 \leftrightarrow F = 15/2,\ m_F = -5/2$

II $F = 17/2,\ m_F = -3/2 \leftrightarrow F = 15/2,\ m_F = -3/2$

III $F = 17/2,\ m_F = -5/2 \leftrightarrow F = 15/2,\ m_F = -5/2$

Fig. VI-21. Direct transitions and $\Delta F = 0$ transitions for Er^{163}

is true, then a and b are correlated for that value of magnetic field.

$$\S = \frac{\partial F/\partial a}{\partial F/\partial b} \approx -\frac{b}{a} \quad \text{where } F = \text{transition frequency} \qquad (6.2)$$

For $a = 314$ and $b = -6220$; $\partial F/\partial a = -0.374$, $\partial F/\partial b = -0.0181$ for $F = 17/2$ at 125 guass which gives $\S = 20.6 \approx 19.8$; for $F = 15/2$ at 125 gauss one gets $\S = 19.5$. If one goes up to a high enough magnetic field the correlation would become negligible. For $F = 17/2$ at 400 guass $\S = 24.4$.

The results are

$$I = 5/2$$
$$a = \pm 314(13) \text{ MHz}$$
$$b = \mp 6220(252) \text{ MHz}$$
$$b/a = -19.80(20)$$

Ali's values for Er^{165} are (ALI 64)

$$a = \pm 195(6) \qquad I = 5/2$$
$$b = \mp 3502(115)$$
$$\mu = \pm .652(29)$$
$$Q_{uncorr} = \pm 2.22(6)$$

Using the Fermi-Segrè relations [Eqs. (3.9) and (3.14)] with Er^{165} one obtains for Er^{163}

$$\mu_I(\text{uncorr}) = +1.1(1) \text{ nm}$$
$$Q(\text{uncorr}) = +3.9(5) \text{ barns}$$

where the sign of Q has been chosen positive since most isotopes in this region ($150<A<190$) have positive quadrupole moments, thus fixing the sign of μ_I. No diamagnetic or Sternheimer corrections have been applied.

From Eqs. (4.2) and (4.3) and Q = 3.9 barns one obtains $\delta = 0.37$. According to the Nilsson model one should get a deformation of about $\delta = 0.26$ so the measured value is much too high for the theory. Nilsson feels that a deformation of $\delta = 0.37$ can't be correct (NIL 67) but the data gives this value. If one used $\delta = 0.30$ (the largest value for δ in Nilsson's tables) one gets $Q_{calc} = 3.0$, about 23% below the value calculated from the measured interaction constant b .

From Eq. (4.1) with $g_R = Z/A$, $g_\delta(n) = -3.826$ and $g_\ell = 0$, for $\delta = 0.3$ one obtains $\mu_{calc} = +1.2$ which is 9% above the value obtained from a .

The deformation $\delta = 0.37$ is much too large to agree with the Nilsson model so something is in error, either the model or the data. I personally feel that in this case the model is in error and needs correction.

ACKNOWLEDGEMENTS

The completion of this work was made possible only through the assistance of many persons. I would especially like to thank:

Professor R. Marrus for his guidance in all aspects of the research.

Professor H. Shugart for his interest and suggestions.

Dr. A. Ramsey for assisting in the experimental runs.

Mrs. J. Taylor for typing the thesis.

The members of the Lawrence Radiation Laboratory Health Chemistry Department for their aid in scheduling and handling the radioactive isotopes, expecially E. Calhoon.

My mother for her patience throughout my research.

This work was performed under the auspices of the U. S. Atomic Energy Commission.

REFERENCES

ALI 64 D. E. Ali, Spin of Gd^{153}, Dy^{159}, and Pm^{148} and Hyperfine Structure of Pm^{148} and Er^{165}, (Ph.D. Thesis), University of California Radiation Laboratory Report UCRL-11536, June 1964. (unpublished)

BAK 60 F. S. Baker, Graphs and Tables of Zero Field Hyperfine Structure Level Ordering in Free Atoms, Lawrence Radiation Laboratory Report UCRL-9364, August 1960.

BLE 64 B. Bleamey, Nuclear Moments of the Lanthanons, Proceedings of the Third International Congress on Quantum Electronics, P. Grivet and N. Bloemberger, Ed. (Columbia University Press, New York, 1964).

BOH 53 A. Bohr and B. R. Mottelson, Collective and Individual Particle Aspects of Nuclear Structure, Dan. Mat. Fys. Medd. 27, 16 (1953).

BRI 57 G. O. Brink, Nuclear Spin of Thallium-197, Thallium-198m, Thallium-199 and Thallium-204, (Ph.D. Thesis), University of California Radiation Laboratory Report UCRL-3642, June 1957. (unpublished)

CAB 60 A. Y. Cabezas, Electronic and Nuclear Properties of Some Radioactive Rare-Earth Elements, (Ph.D. Thesis), University of California Radiation Laboratory Report UCRL-9346, August 1960. (unpublished)

CHI 61 L. -W. Chiao, The Magnetic Properties of Deformed Nuclei, (Ph.D. Thesis), University of California Radiation Laboratory Report UCRL-9648, April 1961. (unpublished)

CON 35 E. V. Condon and G. H. Shortley, Theory of Atomic Spectra, (Cambridge University Press, London 1935).

DOY 63 W. M. Doyle, Hyperfine-structure Studies of Er^{169} and Isotopes of Refractory Elements, (Ph.D. Thesis), University of California Radiation Laboratory Report UCRL-10609, January 1963. (unpublished)

DUN 11 L. Dunoyer, Compt. Rend. 152, 594 (1911).

MAR 62 R. A. Marrus and W. A. Nierenberg, On Atomic Beams, in Proceedings of the International School of Physics, Enrico Fermi, Course XVII, August 1960. (Academic Press, New York, 1962) pp. 118-156.

MAY 55 M. G. Mayer and J. H. D. Jensen, Elementary Theory of Nuclear Shell Structure, (J. Wiley & Sons, Inc., New York 1955).

MOT 59 B. R. Mottelson and S. G. Nilsson, The Intrinsic States of Odd-A Nuclei Having Ellipsoidal Equilibrium Shape, Mat. Fys. Shr. Dan. Vid. Selsk. 1, 8 (1959).

NIE 57 W. A. Nierenberg, The Measurement of the Nuclear Spins and Static Moments of Radioactive Isotopes, An. Rev. Nuc. Sci. 7, (1957).

NIL 55 S. G. Nilsson, Binding States of Individual Nucleons in Strongly Deformed Nuclei, Dan. Mat. Fys. Medd. 29, 16 (1955).

NIL 67 S. G. Nilsson (University of California, Berkeley) private communication 1967.

PEN 64 S. Penselin (University of Bonn, Germany), private communication with H. S. Shugart, 1964.

RAB 38 I. I. Rabi, J. R. Zacharias, S. Millman, and P. Kusch, Phys. Rev. 53, 318 (1938).

RAM 56 N. F. Ramsey, Molecular Beams, (Oxford University Press, London 1956).

SHU 66 H. A. Shugart, Hyperfine F2, University of California, 1966. (unpublished)

SLA 60 J. C. Slater, Quantum Theory of Atomic Structure, Vol. II, (McGraw Hill, New York, 1960).

SMI 51 K. F. Smith, Nature 167, 942 (1951).

SMI 61 K. F. Smith and I. J. Spaulding, Proc. Roy. Soc. (London) A265, 133 (1961).

STE 21 O. Stern, Z. Physik 7, 249 (1921).

ZAC 42 J. R. Zacharias, Phys. Rev. 61, 270 (1942).

ZUR 64 D. H. Zurlinden, Atomic Research on Radioactive Atoms, Hyperfine 4, University of California, September 1964. (unpublished)